MAPPING OF ANNUAL ICE LAYER EXTENT AND SNOW ACCUMULATION IN THE PERCOLATION ZONE OF THE GREENLAND ICE SHEET: QUICKSCAT APPLICATION AND GREENLAND CLIMATE NETWORK

Konrad Steffen, Thomas Philips, John Adler, Kevin Sampson, William Colgan

University of Colorado at Boulder
Cooperative Institute for Research in Environmental Sciences
Campus Box 216, Boulder CO 80309

NASA Grant NNG06GB08G

Progress Report
to
National Aeronautics and Space Administration, Cryospheric Program and
National Science Foundation, Office of Polar Programs

January 2008

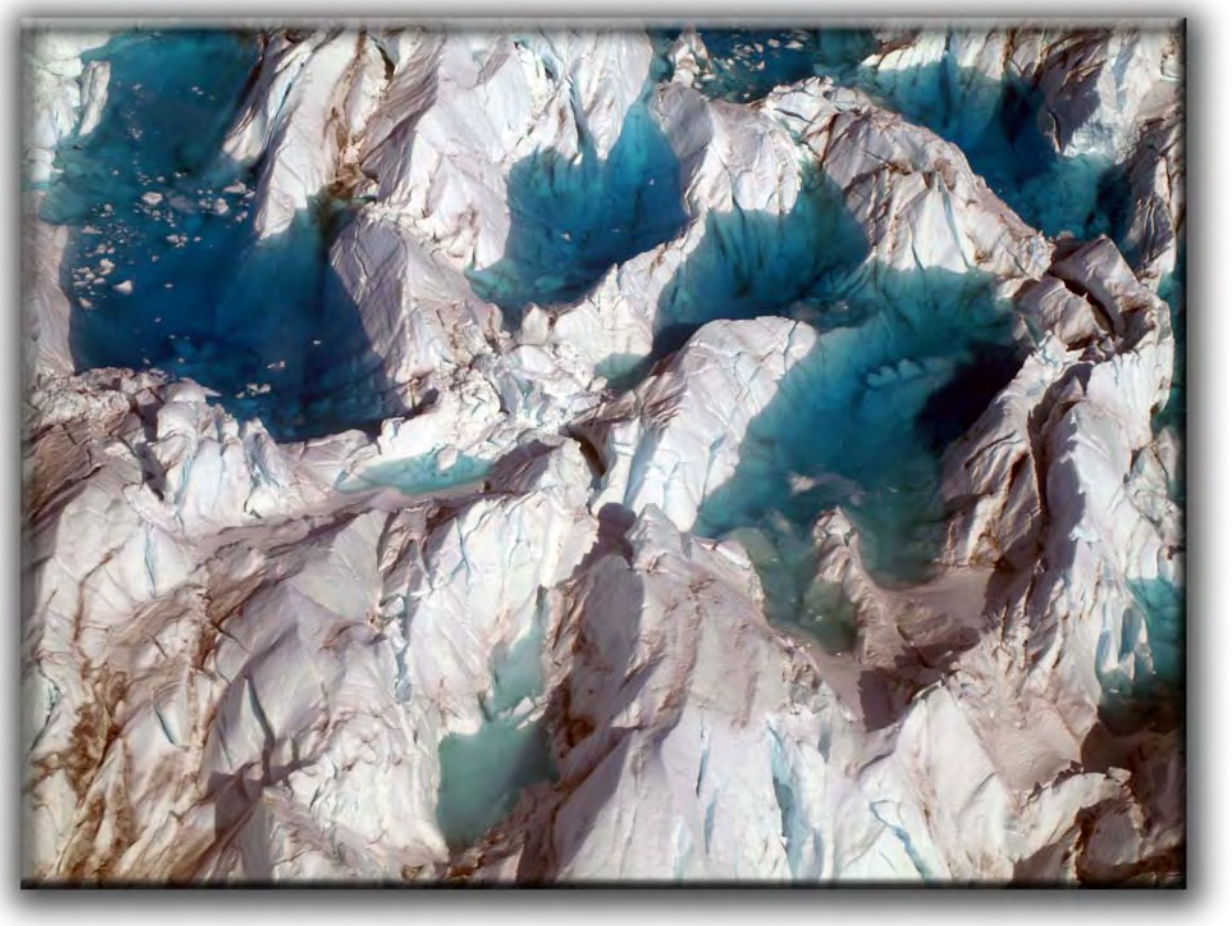

CREVASSES IN LOWER PART OF JAKOBSHAVN ISBRAE FILLED WITH WATER

TABLE OF CONTENTS

TABLE OF CONTENTS 2

1. Field Expedition 2007 3

1.1 Logistic Summary 3
1.2 Automatic Weather Station Maintenance 4
1.3 Personal 5

2. Greenland Climate Network (GC-Net) 6

2.1 Overview 6
2.2 GC-Net Users 6
2.4 Updated Swiss Camp Climatology 9
2.5 Updated PM Melt Climatology 10
2.5 GC-Net Citation List 11

3. Results 14

3.1 Shallow Firn Layer Climatology 14
3.1.1 Abstract 14
3.1.2 Data 14
3.1.3 Firn compaction modelling 15
3.1.4 Correction of simultaneous temperature variations 17
3.1.6 Firn temperature 19
3.2. Modeling of Englacial Hydrology 21
3.2.1. Introduction 21
3.2.2. Motivation 21
3.2.3. Source of water 21
3.2.4. West Greenland temperature profile 23
3.2.5. Modelling sub- and englacial conduits 24
3.2.6. Preliminary results for melt 26
3.3 Influence of Meltwater on Greenland Ice Sheet Dynamics 27
3.3.1 An overview of the importance of water in ice dynamics 27
3.3.2 Evidence of subglacial water in the Greenland Ice Sheet 30
3.3.3 An introduction to the Swiss Camp Regional Model 31
3.4 UAS over the Greenland Ice Sheet 33
3.4.1 Overview 33
3.4.2 Data collection platforms 34
3.4.3 Sensors 35
3.4.4 Data discussion 35
3.4.5 Conclusions 36
3.4.6 Future research 37

4. Proposed Field Activities and Research Objectives 2008 38

4.1 AWS Maintenance 38
4.2 GPS Network Maintenance 38
4.3 Ground Penetration Radar 38

5. Bibliography 39

1. Field Expedition 2007

1.1 Logistic Summary

Date	Location	Work
April 2007		
22	Scotia-SFJ	Team members (Steffen, Adler,Philips) and cargo on C-130
24	SFJ-Saddle-NASA SE	AWS maintenance and download, overnight
25	NASA SE-DyeII-SFJ	AWS maintenance and download Overnight
26	SFJ- SC - SFJ	Cargo and flight to N70, CP, Up50 download
27	SFJ – S Dome – SFJ	AWS download and tower extended
May 2007		
2	SFJ – Thule	Stat of northern AWS traverse
3	Thule-GITS-NEEM	AWS maintenance
3	-HUM-Thule	AWS maintenance
4	Thule Pet. ELA – SFJ	AWS download
6	SFJ-SC-SFJ	Swiss camp put in
7	SC	Ice thermistor download
9	SC	10 m tower, radiation tower, AWS download
9	SC	Snow survey (107 cm mean snow), 0 m melt of ice
10	JAR1/2	AWS download
11	SC	*Polar Palooza film team arrives* (3 days)
14	SC	*National Geog. film team visit* (3 days)
15	JAR1	Re-drilling AWS
17	SC	*3 radio stations reps. arrive (*5 days)
22	N70, UP50	work on GPS stations
22	SC	*Documenta film team arrives* (3 days)
23	Moulin	GPS profiles
24	SC	*1st CNN team arrives for 6 days*, 1st TV report from SC
25	SC	*2nd CNN team arrives* (Cooper)
26	JAR2	Moulin filming and AWS work
27	SC	*Nancy Pelosi and cong. Committee visits*
27	SC	Both CNN teams leave
28	SC	GPR profiles towards CP1, *NHK film team arrives*
30	Moulin	GPR profiles
June 2007		
1	SC	Download all instrument towers, closing camp
6	SC	Swiss Camp pull-out

1.2 Automatic Weather Station Maintenance

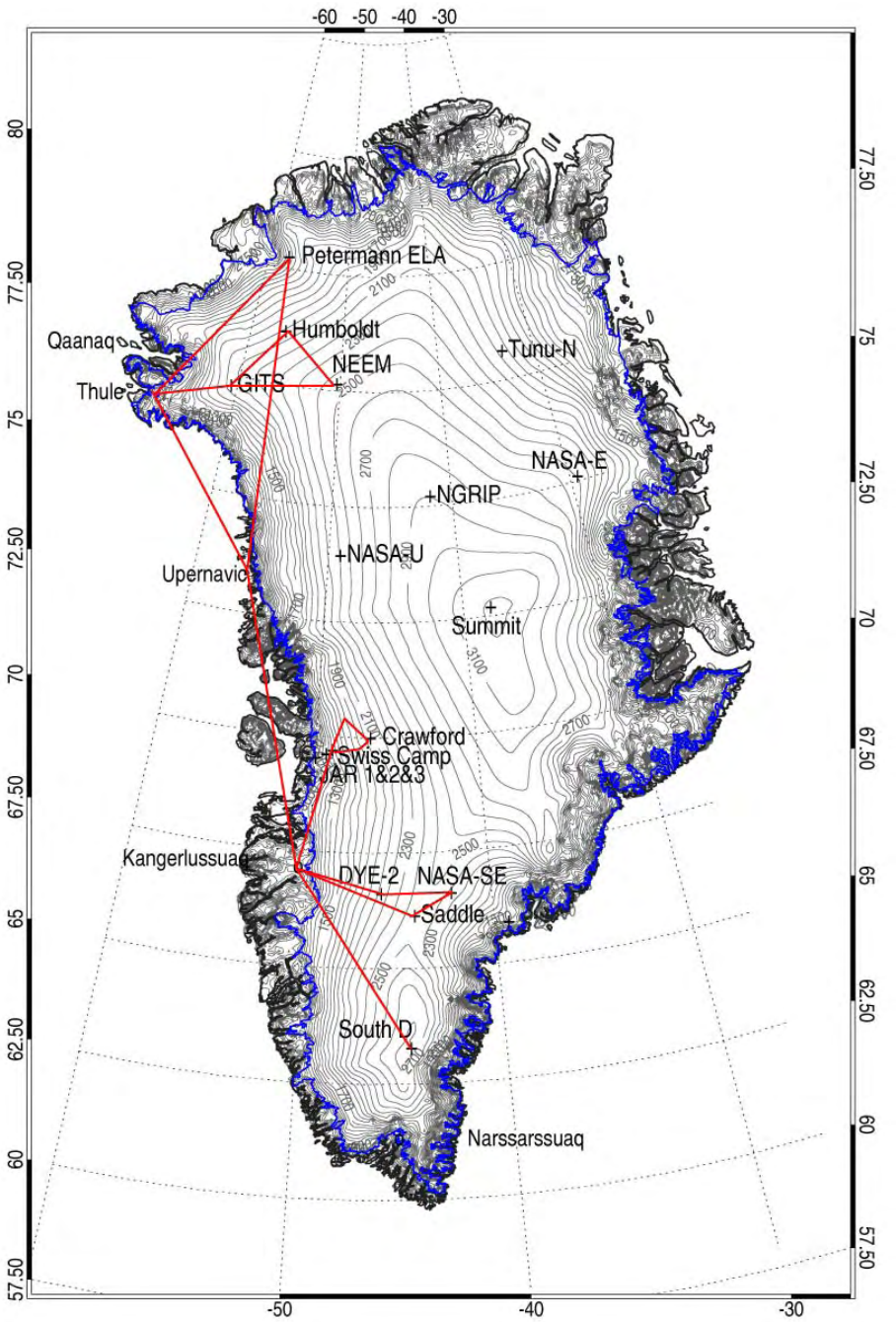

Figure 1.2.1: Greenland Climate Network (GC-Net) automatic weather stations as of summer 2006. The red arrows indicate the Twin Otter flight path for the AWS maintenance described in the logistic summary.

1.3 Personal

Name	Institution	Arr.	Dep.
AWS support and Swiss Camp research			
Konrad Steffen	CU-Boulder	4/22	6/7
Kevin Sampson	CU-Boulder	4/22	6/7
John Adler	CU-Boulder	4/22	5/11
Steve Nerem	CU-Boulder	5/5	5/11
Eric Rignot	NASA-JPL	5/1	5/4
Jay Zwally	NASA-GSFC	5/5	6/7
Jose Rial	Univ. North Carolina	5/5	6/7
Seelye Martin	NASA HQ	5/5	5/7
Moulin Experiment			
Konrad Steffen	CU-Boulder	8/19	8/25
Alberto Behar	NASA-JPL	8/19	8/25
Russ Huff	CU-Boulder	8/19	8/25
John Adler	CU-Boulder	8/19	8/25
Media Visits			
Polar Palooza film team, 2 people		5/11	5/14
National Geog. film team, 4 people		5/14	5/17
Reuters (1 person)		5/17	5/19
Swiss Info (1 person)		5/17	5/22
German radio (1 person)		5/17	5/22
Documenta filmteam (4 person)		5/22	5/24
1st CNN team (3 people)		5/24	5/27
1st CNN team (3 people)		5/25	5/27
NHK film team (4 people)		5/28	6/2
Congressional Visits			
Speaker of the House Nancy Peloci		5/27	5/27
Congressman Ed Markey and wife		5/27	5/27
Congressman Hobsen		5/27	5/27
Congress press person		5/27	5/27

2. Greenland Climate Network (GC-Net)

2.1 Overview

The GC-Net currently consists of 17 automatic weather stations and four smart stakes distributed over the entire Greenland ice sheet (Figure 1.2.1). Four stations are located along the crest of the ice sheet (2500 to 3200 m elevation range) in a north-south direction, Eight stations are located close to the 2000 m contour line (1830 m to 2500 m), and four stations are positioned in the ablation region (50 m to 800 m), and two stations are located at the equilibrium line altitude at the west coast and in the north.). The smart stakes were introduced in spring 2001 to measure the climate in the ablation region in the Jakobshavn area (SMS1-4).

The GC-Net was established in spring 1995 with the intention of monitoring climatological and glaciological parameters at various locations on the ice sheet over a time period of at least 10 years. The first AWS was installed in 1990 at the Swiss Camp, followed by four AWS in 1995, four in 1996, five in 1997, another four in 1999, one in 2002 one in 2003, and the latest one at NEEM in support for the new deep ice core in 2006. Our objectives for the Greenland weather station (AWS) network are to measure daily, annual and interannual variability in accumulation rate, surface climatology and surface energy balance at selected locations on the ice sheet, and to measure near-surface snow density at the AWS locations for the assessment of snow densification, accumulation, and metamorphosis.

In addition to providing climatological and glaciological observations from the field, further application of the GC-Net data include: the study of the ice sheet melt extent (Abdalati and Steffen, 2001); estimates of the ice sheet sublimation rate (Box and Steffen, 2001); reconstruction of long-term air temperature time series (Shuman at al., 2001), assessment of surface climate (Steffen and Box, 2001), and the interpretation of satellite-derived melt features of the ice sheet (*Nghiem et al.,* 2001). Potential applications for the use of the GC-Net data are: comparison of in-situ and satellite-derived surface parameters, operational weather forecast; validation of climate models; and logistic support for ice camps and Thule AFB.

2.2 GC-Net Users

During the last 12 month we received 60 new GC-Net data request and distributed the data using the new Web interface. This web interface allows us to capture the email and affiliation of all GC-Net users, including a short description of their use of the Greenland Climate data. The data request is processed on a UNIX 4-processor workstation and the data is transferred on a FTP site for direct downloading. We will continue top maintain the main portal for all GC-Net data distribution, the main radon being the frequent data reprocessing to increase data quality.

In the following the latest 60 users of GC-Net data are listed by email, name and affiliation since January 2007. They all used the web-based interface (given below) to request the Greenland climate data for model validation, process studies, satellite comparison, and more.

Home page of GC-Net and web interface for data request:
http://cires.colorado.edu/science/groups/steffen/gcnet/

Greenland Climate Network Data Request

ID	Email	Name	Organization
141	mcathles@uchicago.edu	Mac Cathles	University of Chicago
142	syuksel@turkak.org.tr	Salih Yuksel	Middle East Technical University
143	bernhard@biospherical.com	Germar Bernhard	Biospherical Instruments
144	bernhard@biospherical.com	Germar Bernhard	Biospherical Instruments
145	thorben.dunse@geo.uio.no	Thorben Dunse	Dep. of Geosciences, University of Oslo
146	lisa.ho@colorado.edu	lisa ho	CIRES
147	fxsm@uaf.edu	Sebastian H. Mernild	University of Alaska Fairbanks
148	fxsm@uaf.edu	Sebastian H. Mernild	University of Alaska Fairbanks
149	marc.simard@jpl.nasa.gov	Marc Simard	JPL
150	thorben.dunse@geo.uio.no	Thorben Dunse	Dep. of Geosciences, University of Oslo
151	toverly@cresis.ku.edu	Thomas Overly	Center for Remote Sensing of Ice Sheets
152	nhealey@bigred.unl.edu	natehealey	university of nebraska, lincoln
153	justin.bobak@nrl.navy.mil	Justin Bobak	Naval Research Laboratory
154	shun-li@atmosp.physics.utoronto.ca	Shunli Zhang	Dep. of Physics, University of Toronto
155	shun-li@atmosp.physics.utoronto.ca	Shunli Zhang	Dep. of Physics, University of Toronto
156	shun-li@atmosp.physics.utoronto.ca	Shunli	University of Toronto
157	carl.egede.boggild@unis.no	Carl Egede Bøggild	UNIS
158	v.l.parry@sms.ed.ac.uk	Vicki Parry	University of Edinburgh
159	rxp245@psu.edu	Rui Peng	Penn State University
160	rxp245@psu.edu	Rui Peng	Penn State University
161	rxp245@psu.edu	Rui Peng	Penn State University
162	rxp245@psu.edu	Rui Peng	Penn State University
163	rxp245@psu.edu	Rui Peng	Penn State University
164	rxp245@psu.edu	Rui Peng	Penn State University
165	"Indrajit Bhattacharya"	Indrajit Bhattacharya	Ohio State
166	thersonly1stevie@hotmail.com	Stevie Mendham	
167	edwer.veldhuijzen@grontmij.nl	Edwer Veldhuijzen	
168	v.l.parry@sms.ed.ac.uk	Vicki Parry	University of Edinburgh
169	twilap@u.washington.edu	Twila Moon	University of Washington
170	vivienne.raper@bristol.ac.uk	Vivienne Raper	Bristol Glaciology Centre
171	rsf@geus.dk	Robert Fausto	Geological survey of Denmark and Greenland (GEUS)

172	olibaur@gmx.de	Oliver Baur	Curtin University of Technology, Perth, Australia
173	g.n.petersen@uea.ac.uk	Gudrun Nina Petersen	University of East Anglia, UK
174	g.n.petersen@uea.ac.uk	Gudrun Nina Petersen	University of East Anglia, UK
175	xchen@nju.edu.cn	Xing Chen	Nanjing University
176	mas@dmi.dk	Martin Stendel	Danish Meteorological Institute
177	bailesheng@hotmail.com	Lesheng Bai	Polar Research Center. OSU
178	JRumrill	Julie Rumrill	University of Vermont
179	kindig@nsidc.org	Dave kindig	NSIDC
180	david.schuler@umontana.edu	David Schuler	University of Montana
181	shun-li@atmosp.physics.utoronto.ca	Shunli Zhang	University of Toronto
182	edwer.veldhuijzen@grontmij.nl	Edwer Veldhuijzen	
183	fxsm@uaf.edu	Dr. Sebastian Mernild	University of Alaska Fairbanks
184	fxsm@uaf.edu	Dr. Sebastian Mernild	University of Alaska Fairbanks
185	sebastien.descamps@uqar.qc.ca	Descamps	UQAR
186	bertw@deos.tudelft.nl	Wouters	Delft University of technology
187	twilap@u.washington.edu	Twila Moon	University of Washington
188	Jun.Li@nasa.gov	Jun Li	SGT/GSFC
189	jun.li@nasa.gov	Jun Li	SGT/GSFC
190	mmcmill1@staffmail.ed.ac.uk	Malcolm McMillan	University of Edinburgh
191	Taneil.Uttal@noaa.gov	Taneil Uttal	NOAA
192	jun.li@nasa.gov	Jun Li	SGT/GSFC
193	Larry.V.Stock@nasa.gov	Larry Stock	NASA, Cryospheric Sciences Branch, Code 614.1
194	bhattacharya.21@osu.edu	Indrajit	BPRC , OSU
195	jun.li@nasa.gov	Jun Li	SGT/GSFC
196	jun.li@nasa.gov	Jun Li	GSFC
197	carolinejlarsen@gmail.com	Carrie Larsen	The Ohio State University
198	JRumrill@uvm.edu	Julie Rumrill	University of Vermont
199	joey@ucar.edu	Joey Comeaux	NCAR
200	joey@ucar.edu	Joey Comeaux	NCAR
201	460931@swan.ac.uk	Nick Selmes	University of Swansea UK (Glaciology Group/GLIMPS)

2.4 Updated Swiss Camp Climatology

The mean annual temperature has increased by 4.3 ºC using a linear regression model as shown in Figure 1.4.1. The minimum temperature in 1992 was the result of the aerosol loading caused by the Mt. Pinatubo eruption. The linear regressing model at 95% confidence shows that the Pinatubo cooling and also the subsequent warming from the mid 90's were outside the 95% level of confidence. The warming that occurred since 2000 to present shows approximately the same trend then the 15-year time series. The warmest mean annual temperature was recorded with -10.3 ºC in 2006. The temperature record for the Swiss Camp 2007 is not available yet but first indications show that it was another record warm year, above all previously recorded values since the beginning of this time series.

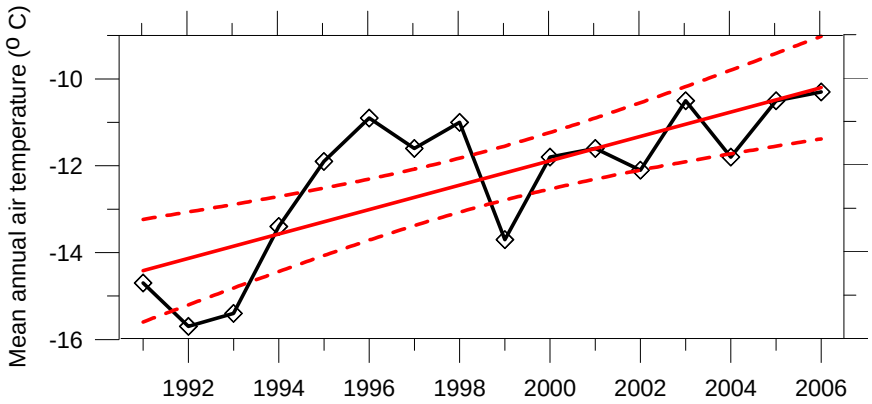

Figure 1.4.1: Swiss Camp mean annual temperature 1991 – 2006 (black line) with a linear regression model (red line) and 95% confidence levels (dashed red lines).

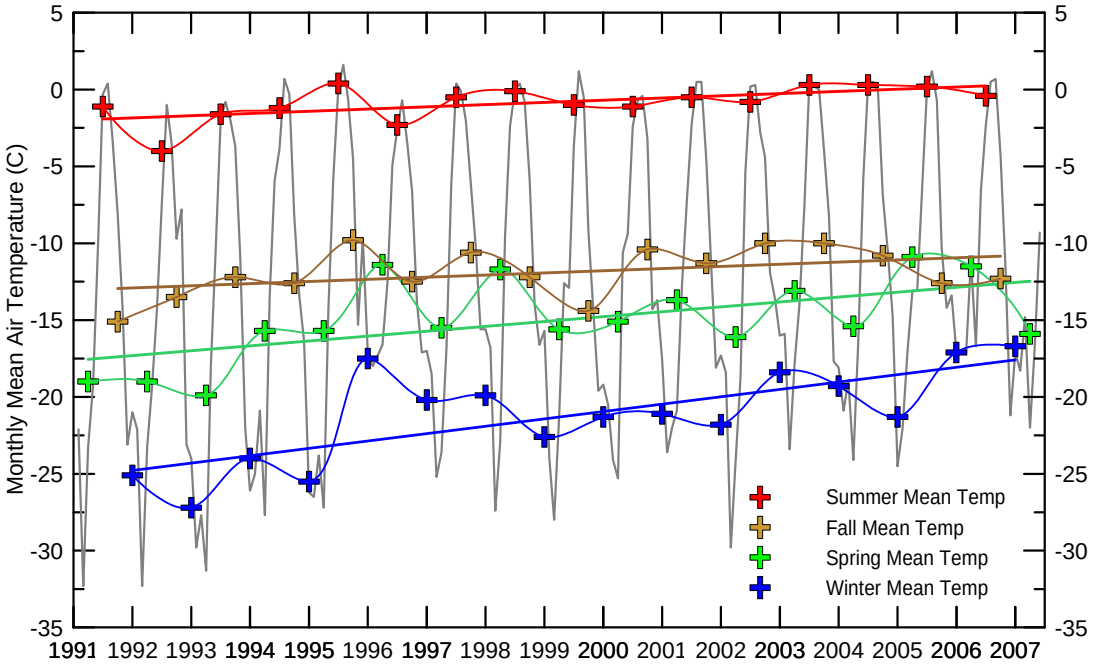

Figure 1.4.2: Air temperature variability and trend for Swiss Camp, 1991 to 2006.

The statistical analysis of the Swiss Camp air temperature record reveals large interannual variability in all seasons with increasing temperatures throughout the recording period (Fig. 1.4.2). The mean spring temperature increased from -17.5 ºC to -12.5 ºC, and fall temperature increased from -12.7 ºC to -11.0 ºC between 1991 and 2007, using a linear model. The winter temperature showed the largest increase of 6.3 ºC, whereas summer temperatures increased 2.3 ºC during the 16 years (1991 – 2006). The climate record at Swiss Camp shows a clear warming trend that started around 1995, consistent with the Arctic warming.

2.5 Updated PM Melt Climatology

The annual melt signal since 1979 is highly variable with a standard deviation that is 28% of the mean (Fig. 1.5.1). Error bars on the annual total melt area are computed for the first time based on the GC-Net air temperature record. The total melt area in Greenland has increased at a rate of 1.4% per year since 1979 (91% significant.) The melt signal is highly periodic repeating every 3 or 4 years. The record melt year occurred in 2007 and lies 10% above the previous record melt year of 2005. The 1992 melt year, following the Mt. Pinatubo eruption, is the minimum melt year on record at 2 standard deviations below the mean followed closely by 1996 (1.6 standard deviations below the mean.) Peak melt occurs, on average, on August 1st. Increasing trends during July (1.7% per year, 90% significant) and August (1.9% per year, 95% significant) are largely responsible for the overall annual trend (Fig. 1.5.1). The onset and duration of the melt season have not changed significantly.

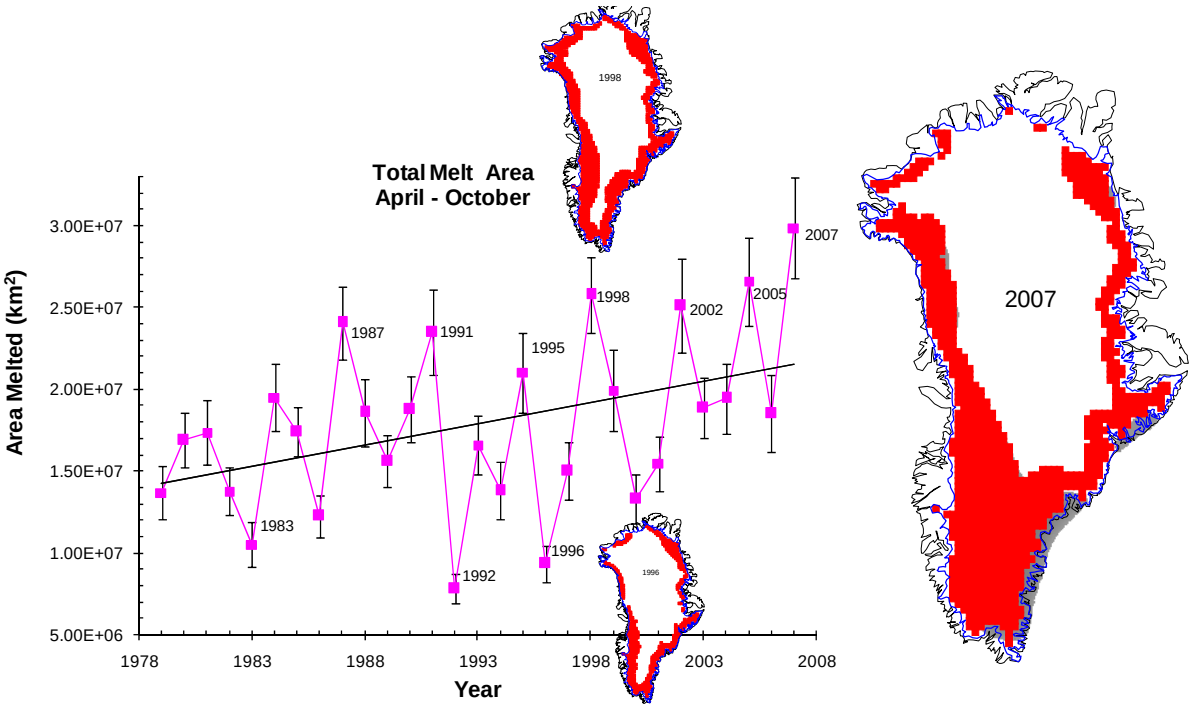

Figure 1.5.1: Melt climatology for the Greenland ice sheet derived from passive microwave satellite data for 1979 – 2007. Note that the 2007 cumulative annual melt area was 10% higher than the previous record in 2005.

2.5 GC-Net Citation List

This list represents publications that made use of Greenland Climate Network (GC-Net) data.

Abdalati, W. and K. Steffen, Greenland ice sheet melt extent: 1979-1999, J. Geophys. Res., 106(D24), 33,983-33,989, 2001.

Box, J.E., D.H. Bromwich1, B.A. Veenhuis, Le-S. Bai, J.C. Stroeve, J.C. Rogers, K. Steffen, T. Haran, S.-H.. Wang, Greenland ice sheet surface mass balance variability (1988-2004) from calibrated Polar MM5 output, J.Clim., 2005.

Box, J. E., Surface Water Vapor Exchange on the Greenland Ice Sheet Derived from Automated Weather Station Data, PhD Thesis, Department of Geography, University of Colorado, Boulder, CO, Cooperative Institute for Research in Environmental Sciences, 190 pp, 2001.

Box, J.E. and K. Steffen, Sublimation on the Greenland ice sheet from automated weather station observations, J. Geophys. Res., 106(D24), 33,965-33,982, 2001.

Bromwhich, D., J. Cassano, T. Klein, G. Heinemann, K. Hines, K. Steffen and J. Box, Mesoscale modeling of katabatic winds over Greenland with Polar MM5, Mon. Weather Review, 129, 2290-2309, 2001.

Cassano, J.J., J.E. Box, D.H. Bromwich, L. Li, and K. Steffen, Evaluation of Polar MM5 simulations of Greenland's atmospheric circulation, J. Geophys. Res., 106(D24), 33,867-33,890, 2001.

Cullen, N., and K. Steffen, Unstable near-surface boundary conditions in summer on top of the Greenland ice sheet., Geophys. Res. Lett., 28(23), 4491-4494, 2001.

Cullen, N.J., K. Steffen, and P. D Blanken, Nonstationarity of Turbulent Heat Fluxes at Summit, Greenland, Boundary-Layer Meteorology, DOI 10.1007/s10546-006-9112-2, 2006.

Davis, C.H. and D.M. Segura, An algorithm for time-series analysis of ice sheet surface elevations from satellite altimetry, IEEE Transactions on Geoscience & Remote Sensing, 39(1), 202-206, 2001.

Dassau, T.M., A. Sumer, S. Koeniger, P. Shepson, J. Yang, R. Honrath, N. Culen, K. Steffen, Investigation of the role of the snowpack on atmospheric formaldehyde chemistry at Summit, Greenland, J. Geophys. Res., 107(D19), ACH 9.1-14, 36, 2595-2608, 2002.

Hanna , E., P. Huybrechts, K. Steffen, J. Cappelen, R. Huff, Ch. Shuman, T. Irvine-Fynn, S. Wise, and M. Griffiths. Increased runoff from melt from the Greenland Ice Sheet: a response to global warming. J. Climate, in press, 2008.

Hanna,H., P.Huybrechts, I. Janssens, J..Cappelen, K. Steffen, and A. Stephens, Runoff and mass balance of the Greenland ice sheet: 1958–2003, J. Geophys. Res., 110, D13108, doi:10.1029/2004JD005641, 2005.

Hanna, E. and P. Valdes, Validation of ECMWF (re)analysis surface climate data, 1979-1998, for Greenland and implications for mass balance modeling of the Ice Sheet, Intern. J. Clim., 21, 171-195, 2001.

Helmig, D, J. Boulter, D. David, J. Birk, N. Cullen, K. Steffen, B. Johsnon, S. Oltmans, Ozone and meteorological boundary-layer conditions at Summit, Greenland, Atm. Environm., 36, 2595-2608, 2002.

Herzfeld, U.C., J.E. Box, K. Steffen, H. Mayer, N. Caine, and M. Losleben, A case study on the influence of snow and ice surface roughness on melt energy, Zeitschrift für Gletscherkunde und Glazialgeology, 39, 1-42, 2006.

Honrath, R.E. Y.Y. Lu, M.C. Peterson, J.E. Dibb, M.A. Arseault, N.J. Cullen, and K. Steffen. Vertical fluxes of NOx, HONO, and HNO3 above the snowpack at Summit, Greenland. Atm. Environm, 36, 2629-2640, 2002.

Klein, T., G. Heinemann, D. H. Bromwich, J. J. Cassano and K. M. Hines, Mesoscale modeling of katabatic winds over Greenland and comparisons with AWS and aircraft data, J. Met. Atmos. Phys., 8(1/2), 115-132, 2001.

Klein, T., G. Heinemann, Simulations of the katabatic wind over the Greenland ice sheet with a 3D model for one winter month and two spring months, Report of the DAAD/NSF project 315-PP, 1999.

Mernild, S., G. Liston, Ch. Hiemstra, and K. Steffen. Surface melt area and water balance modeling on the Greenland ice sheet 1995-2005. Geophys. Res. Lett., in press 2007.

Mosley-Thompson, E., J.R. McConnell, R.C. Bales, Z. Li, P.-N. Lin, K. Steffen, L.G. Thompson, R. Edwards, D. Bathke, Local to regional-scale variability of annual net accumulation on the Greenland ice sheet from PARCA cores, J. Geophys. Res., 106 (D24), 33,839-33852, 2001.

Murphy, B. F., I. Marsiat and P. Valdes, Simulated atmospheric contributions to the surface mass balance of Greenland. J. Geophys. Res., 106, submitted, 2001.

Nghiem, S.V., , K. Steffen, G. Neumann, and R. Huff, Snow Accumulation and Snowmelt Monitoring in Greenland and Antarctica, International Association of Geodesy Publication, Dynamic Planet , Chapter 5, 31-38, 2007.

Nghiem,S,V., K. Steffen, G. Neumann, and R. Huff, Mapping of ice layer extent and snow accumulation in the percolation zone of the Greenland ice sheet, J. Geophys., Res., 110, F02017, doi:10.1029/2004JF000234, 2005.

Nghiem, S.V., K. Steffen, R. Kwok, and W.Y. Tsai, Diurnal variations of melt regions on the Greenland ice sheet, J. Glaciol., 47(159), 539-547, 2001.

Nolin, A. and J. Stroeve, The Changing Albedo of the Greenland Ice Sheet: Implications for Climate Change, Annals of Glaciology, 25, 51-57, 1997.

Orr, A., E. Hanna, J. Hunt, J. Cappelen, K. Steffen and A. Stephens, Characteristics of stable flow over southern Greenland, *Pure and Applied Geophysics* (PAGEOPH), 161(7), 2004.

Painter, T.H., N.P. Molotch, M. Cassidy, M. Flanner, and K. Steffen, Contact spectroscopy for determination of stratigraphy of snow grain size, *J. Glaciol*, 53(180) 121-127, 2007.

Parry, V., P. Mair, J. Scott, B. Hubbard, K. Steffen, and D. Wingham, Investigations of meltwater refreezing and density variations in the snowpack and firn within the percolation zone of the Greenland Ice Sheet, Ann. Glaciol., 46, 621-68, 2007.

Serreze, M., J. Key, J. Box, J. Maslanik, and K. Steffen, A new monthly climatology of global radiation for the Arctic and comparison with NCEP-NCAR reanalysis and ISCCP-C2 field, J. Climate, 11, 121-136, 1998.

Shuman, C., K. Steffen, J. Box, and C. Stearn, A dozen years of temperature observations at the Summit: Central Greenland automatic weather stations 1987-1999, J. Appl. Meteorol., 40(4),741-752, 2001.

Smith, L.C., Y. Sheng, R.R. Foster, K. Steffen, K.E. Frey, and D.E. Alsdorf, Melting of small Arctic ice caps observed from ERS scatterometer time series, Geophys. Res. Lett., 30(20), CRY 2-14, 2003.

Steffen, K., S.V. Nghiem, R. Huff, and G. Neumann, The melt anomaly of 2002 on the Greenland Ice Sheet from active and passive microwave satellite observations, Geophys. Res. Lett., 31(20), L2040210.1029/2004GL020444, 2004.

Steffen, K., and J.E. Box, Surface climatology of the Greenland ice sheet: Greenland climate network 1995-1999, J. Geophys. Res., 106(D24), 33,951-33,964, 2001.

Steffen, K., W. Abdalati, and I. Serjal, Hoar development on the Greenland ice sheet, J. of Glaciology, 45(148), 63-68, 1999.

Steffen, K., J. E. Box and W. Abdalati, Greenland climate network: GC-Net, CRREL, 98-103 pp., 1996.

Stroeve, J., Assessment of Greenland Albedo Variability from the AVHRR Polar Pathfinder Data Set, J. Geophys. Res., 106(D24), 33,989-34,006, 2001.

Stroeve, J., and A. Nolin, 1997. The changing albedo of the Greenland ice sheet: implications for climate modeling, Ann. of Glaciol., 25, 51-57.

Stroeve, J, J. E. Box, J. Maslanik, J. Key, C. Fowler, Intercomparison between in situ and AVHRR Polar Pathfinder-derived surface albedo over Greenland, Remote Sensing of the Environment, 75(3), 360-374, 2001.

Thomas, R., and PARCA instigators, Program for Arctic Regional Climate Assessment (PARCA): Goals, key findings, and future directions, J. Geophys. Res., 106(D24), 33,691-33706, 2001.

Thomas, R.H., W. Abdalati, E. Frederick, W.B. Krabill, S. Manizade, and K. Steffen, Investigation of surface melting and dynamic thinning on Jakobshavn Isbrea, Greenland, J. Glaciol., 49(165), 231-239, 2003.

Wang, L., M. Sharp, B. Rivard, and K. Steffen, Melt duration and ice layer formation on the Greenland ice sheet, 2000-2004, J. Geophys. Res., 112, F04013, doi:10.1029/2007JF000760 2007.

Zwally, H.J. W. Abdalati, T. Herring, K. Larsen, J. Saba, and K. Steffen. Surface melt-induced acceleration of Greenland ice-sheet flow, Science, 297, 218-222, 2002.

3. Results

3.1 Shallow Firn Layer Climatology

3.1.1 Abstract

Measurements of temperature and other climate variables for the Greenland ice sheet are continuously recorded by the Greenland Climate Network (GC-Net) surface meteorological stations. All GC-Net stations are equipped with a string of thermocouple temperature sensors to provide a record of the firn temperature profile as well as surface temperature and snow height change (*dH/dt*) sensors. Thermocouple temperature measurements have a relative accuracy of 0.1 ºC. A subset of six automatic weather stations is chosen that exhibits good spatial and temporal coverage of the extensive, high elevation (>2000m) accumulation regions of the interior of the ice sheet. The procedure to remove simultaneous temperature variations (STVs) in the thermocouples follows a newly developed, physically based data cleaning technique by *Cathles et al.* (2007). This method allows more physical process and parameter information to be extracted from the existing firn temperature data. To account for densification in the firn, and thus movement of the sensors relative to one another, a temperature-dependent model of firn densification is used which reproduces the strong seasonal signal in the densification rate of the upper firn. Further, the in situ time series of constant-depth temperatures at various levels are compared with modeled temperatures to validate the use of GC-Net data to estimate heat transfer into the snowpack.

3.1.2 Data

The research presented here focuses on data gathered by automatic weather stations (AWSs), distributed across the ice sheet at various locations and altitudes as part of the Greenland Climate Network (GC-Net; *Steffen et al.,* 1996). The stations were established in 1995 with the intention of exploring the climatology of the Greenland ice sheet (*Steffen and Box,* 2001). Only Stations from the GC-Net were used for this analysis of atmospheric and englacial temperatures due to their distributed spatial coverage, uniform construction, and uniform sensor configuration. The data is collected in a solid-state data logger, and transmitted via satellite to GC-Net researchers. Stations are also visited in regular intervals for maintenance and on-site data acquisition.

The assumption is made that areas which the XPGR method (*Abdalati and Steffen* 1995; 1997; 2001) does not indicate as exhibiting annual melt are in the dry snow zone and experience no melting and low melt intensity during the warm seasons. The AWS sites chosen are Humboldt Gl., Summit, Tunu-N, South Dome, NASA-E, and NGRIP, with site specific information listed in Table 3.1.1. Though South Dome occasionally experiences melt at the surface, the inclusion of this station is important for the representation of the southern GIS in this analysis.

Each GC-Net site is equipped with a string of thermocouples to monitor heat flux in the shallow firn layer near the station. This dataset was originally installed for monitoring the conductive heat flux that describes energy dissipation in the snowpack, and in particular for resolving heat input from latent heat release of refreezing meltwater (*Steffen et al.,* 1996; *Steffen and Box,* 2001). In addition to these applications, trends in firn and SAT can be assessed using this dataset. The instruments used are described in Table 3.1.2.

Data from 12 shallow firn cores (14 - 20 m) and one deep (~150 m) firn core from the regions around two GC-Net AWS stations were also used in this investigation. Six firn cores were retrieved from the Humboldt Gl. region in northwest Greenland (Humboldt Gl., 78.5266º N, 56.8305º W, 1995m) during the spring of 1995 (*Steffen et al*., 1997). Two cores were taken in close proximity to the Humboldt Gl. AWS,

within 5 m of each other, and four were taken at a distance of 25 km to the north, south, east, and west. The Humboldt firn core dataset contains 291 depth-density measurements ranging from 0.68 - 146.35 m depth. Depth-density data is used from seven additional ~15 m firn cores that were taken during the same field season in the Tunu region of northeast Greenland (Tunu-N, 78.0168º N, 33.9939º W, 2020m). The dataset at Tunu features 105 depth-density measurements, taken at depths from 0 - 14.04 m. The cores were drilled within a 100 km^2 area, at 25 and 50 km distance north, east, and west of Tunu-N AWS. The depth-density measurements from these cores were used to validate firn compaction model results.

Table 3.1.1 *Location, altitude, and inception date of GC-Net permanent AWS stations used in this study.*

ID#	Name	Latitude	Longitude	Elev.[m]	Start Date
5	Humboldt Gl.	78.5266	56.8305	1995	1995.47
6	Summit	72.5794	38.5042	3208	1996.37
7	Tunu-N	78.0168	33.9939	2020	1996.38
11	South Dome	63.1489	44.8167	2922	1997.31
12	NASA-E	75.0000	29.9997	2631	1997.34
14	NGRIP	75.0998	42.3326	2950	1997.52

Table 3.1.2. *GC-Net measurements used in this study.*

Parameter	Instrument	Relative Accuracy	Sample Interval	# per station
Air Temperature	CS-500[1] or HMP45[2]	0.1°C	60 sec	2
Air Temperature	Type-E Thermocouple[3]	0.1°C	60 sec	2
Surface Height Change	SR-50[1]	1 mm	10 min	2
Snow Temperature	Type-T Thermocouple[3,4]	0.1°C	15 sec	10

[1] Campbell Scientific, Inc.
[2] Vaisala Inc.
[3] Omega Engineering, Inc.
[4] special limits of error thermocouple

3.1.3 Firn compaction modelling

Variability in the density profile of an ice sheet is due to changes in temperature, accumulation rate, and the density of recently deposited snow near the surface of the ice sheet (*Arthern and Wingham,* 1998). Thus, the dH/dt at time *t* is the sum of accumulation $A(t)/\rho_0$, firn densification $V_{fc}(0,t)$, advection and thinning of ice V_{ice}, and surface ablation $B(t)$, such that

$$\frac{dH(t)}{dt} = \frac{A(t)}{\rho_0} - V_{fc}(0,t) - V_{ice} - B(t).$$

Equation 3.1.1 is identical to Equation 1 in *Zwally and Li* (2002). The term V_{ice} is neglected here because changes in vertical velocity of ice and crustal motion underneath the ice sheet are not observed by the GC-Net acoustic surface height sensor. Though ablation $B(t)$ is incorporated into the dH/dt signal, the term may be neglected in dry zones of the GIS (*Zwally and Li,* 2002). Snow densification and accumulation are incorporated into the dH/dt signal at each time-step, because sub-surface densifica-

tion will act to lower the surface recorded by the sensor. Thus, Equation 3.1.1 is simplified in this analysis to become

$$\frac{dH(t)}{dt} = \frac{A(t)}{\rho_0} - V_{fc}(0,t).$$

Differential firn densification with depth can act to push sensors together and disrupt the even-spacing of the original sensor placement. For these reasons it is necessary to attempt to model densification of snow layers between sensors in the shallow firn to achieve a correct depth-density profile as well as a correct accumulation time-series.

A model intercomparison was created to assess the suitability of different firn compaction models. The models tested were *Schytt* (1958), *Kojima* (1967), *Herron and Langway* (1980), and *Zwally and Li* (2002). The best model for simulating firn compaction based on available GC-Net data is that of *Zwally and Li* (2002). The model allows for the input of surface temperature and dH/dt at each time step, allowing for seasonal temperature variations to cause differential compaction with time. Figure 3.1.1 shows the model reconstruction of *in-situ* firn core data taken from the Humboldt and Tunu regions in northern Greenland.

The model is initialized with a depth-density profile that closely resembles *in-situ* firn core data, and drives sub-surface temperature with the GC-Net recorded surface temperature. The original placement of subsurface thermocouple temperature sensors is input and the densification between layers and depth of each sensor relative to the surface is calculated. Figure 3.1.2 illustrates the relative-depth trajectory of temperature sensors based on firn densification calculated with the *Zwally and Li* (2002) compaction model.

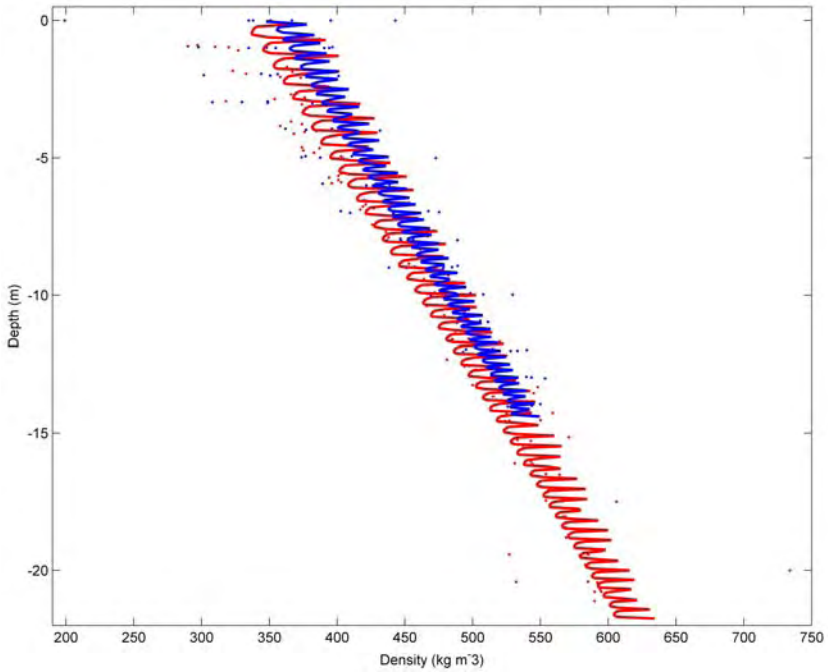

Figure 3.1.1: Best fit curves of ρ(z) based on Zwally and Li (2002) for Humboldt (red line) and Tunu (blue line). Dots represent in-situ firn core data.

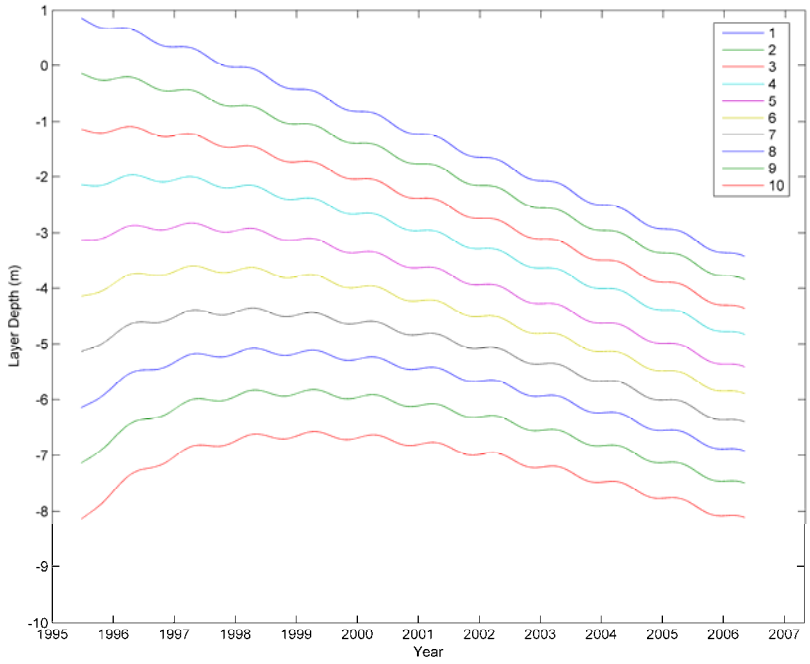

Figure 3.1.2: Depth of each sensor in the GC-Net thermocouple string at Humboldt Gl. AWS relative to the surface. Densification is calculated using Zwally and Li (2002).

3.1.4 Correction of simultaneous temperature variations

Measurement error results from inaccuracies between the temperature measured by the multiplexer near the terminal strips (the reference temperature) and the actual temperature of the reference junction. High-frequency (daily) temperature variations with magnitudes up to 0.20 mV (5.2 °C) occur in the vicinity of the data-logger housing of GC-Net AWS measurements used in this study, which can induce simultaneous temperature variations (STVs) at different depths in a thermocouple temperature profile (*Cathles et al.*, 2007). The variations are described in Table 3.1.3. The causes are likely an uncorrected voltage introduced within the data logger enclosure, wire heating, errors in the reference thermistor, or a temperature-dependent voltage offset produced within the data logger electronics (*Cathles et al.*, 2007). The investigators *in Cathles et al.* (2007) present a simple method for removing STV error, using the deepest (and thus most constant) temperature measurement and applying a correction for simultaneous high frequency variations in all thermocouples above that depth. A smooth curve must be fitted to the temperature time series bearing minimal fluctuation, and the deviation from the smooth curve is used to correct all thermocouples that share the same data logger enclosure. Thus, a running 9th order polynomial is applied to each time step (dt = 1 h), accounting for the six month period before and after each individual measurement. The thermocouple temperatures of both the smoothed polynomial curve and the actual recorded dataset must be converted to voltages using the National Institute of Standards and Technology (NIST) equations (*Burns et al.*, 1993) to obtain the offset voltages (ΔV) necessary to correct the data. The equations for STV correction are as follows:

$$\Delta V = {}_{M}V_{10} - {}_{A}V_{10},$$
$${}_{C}V = {}_{M}V - \Delta V,$$

where ${}_{M}$ indicates the measured voltage (converted from the recorded temperature), ${}_{A}$ indicates the 'actual' voltage (the polynomial that best describes the dataset), and ${}_{C}$ indicates the 'corrected' voltages. Once a dataset of corrected voltages is obtained, the values are converted to temperatures using the NIST equations of *Burns et al.* (1993). The result is a dataset corrected for STV errors.

Uncertainties associated with thermocouple measurement include the influence of natural temperature fluctuations near the reference junction (*Recktenwald*, 2006). Higher quality data can be obtained in the future by keeping the data logger enclosure at a more constant temperature via a heating mechanism or burial within the snowpack (*Recktenwald*, 2006; *Cathles et al.*, 2007). *Recktenwald* (2006) suggests the use of a "zone box" to provide a uniform temperature environment for a group of reference junctions. A study is currently underway by the author at ETH Camp in western Greenland to assess the effect of insulating standard data logger enclosures on high frequency noise in the snow temperature profile datasets. Though the uniform temperature inside the zone box may vary in time, it should do so slowly. Thus, a thick layer of rigid polystyrene insulation is mounted inside an enclosure, surrounding and protecting the reference temperature from high frequency temperature variation.

Table 3.1.3 Voltage and temperature correction statistics.

ID#	Name	ΔV_{max} (mV)	ΔT_{max} (°C)	ΔV_{mean} (mV)	ΔT_{mean} (°C)
5	Humboldt Gl.	-0.1639	-4.2701	±0.0020	±0.0510
6	Summit	-0.1457	-3.795	±0.0066	±0.1720
7	Tunu-N	-0.0674	-1.7523	±0.0045	±0.1171
11	South Dome	-0.0469	-1.2168	±0.0048	±0.1236
12	NASA-E	+0.0358	+0.9264	±0.0039	±0.1020
14	NGRIP	-0.2009	-5.2406	±0.0055	±0.1432

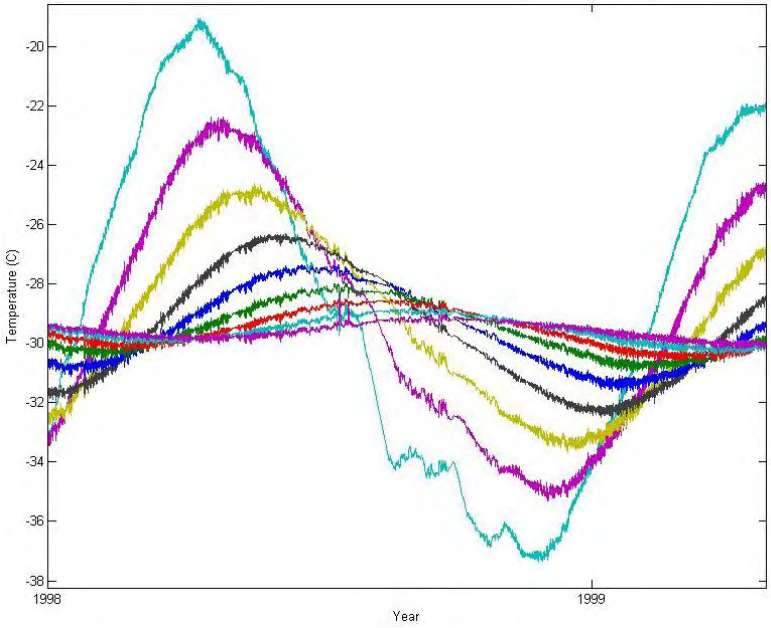

Figure 3.1.3: Measured temperature cycles at 10 depths at NASA-E AWS before STV correction.

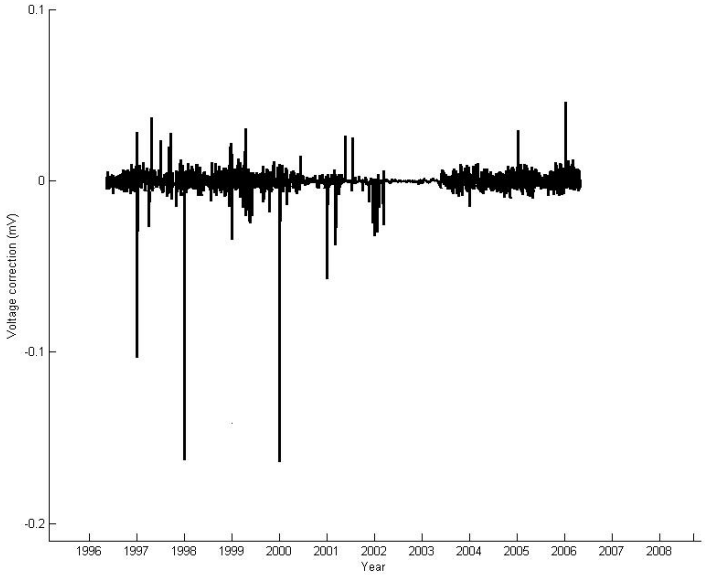

*Figure 3.1.4: Voltage correction (Δ*V*) for the entire Humboldt Gl. AWS thermocouple time series.*

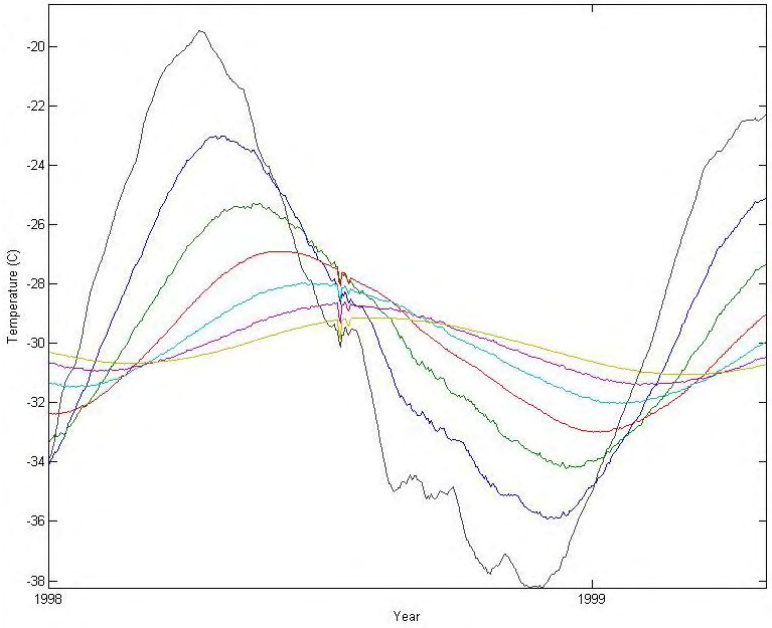

Figure 3.1.5: Measured temperature cycles at 10 depths at NASA-E AWS after STV correction.

3.1.6 Firn temperature

In order to make the dataset more suitable for analysis, the analysis of temperature data must compensate for variations in depth using the initial depth at the time of sensor deployment, and adjusting for the surface height change (dh/dt) that is recorded by the surface height gauges. The problem was noted by *Schytt* (1960) though not corrected.

The depth-correction for the thermocouple sensors is based on the *Zwally and Li* (2002) firn densification model. The model is forced with GC-Net surface temperature, and the sensor depths are initialized based on the depth of sensors at station inception. The model is run forward in time as the depth of each sensor relative to the surface is calculated based on the rate of accumulation and densification. The correct depth-temperature profile is then calculated by linear interpolation between sensors. The sensors begin at 1 m intervals but are pushed together as the snow between them compacts. Thus, the error in interpolation is never more than ½ of the difference of two adjacent sensor temperature values. Because temperature varies little with depth, the error is minimal.

Surface temperature from GC-Net stations for each AWS site in this study are listed in Tables 3.1.4 and 3.1.5. Firn temperature time-series are currently being conducted by GC-Net researchers and results will be available shortly.

Table 3.1.4 GC-Net Surface Temperature measurements

Site	Maximum T	Minimum T	Amplitude*
Humboldt Gl.	June 10	December 9	32.6° C
Summit	July 17	January 15	29.4° C
Tunu-N	July 18	January 16	33.4° C
South Dome	June 10	December 9	21.9° C
NASA-E	July 17	January 15	29.8° C
NGRIP	July 19	January 17	32.1° C

* Peak-to-peak amplitude

Table 3.1.5 GC-Net Surface Temperature statistics

Site	Maximum T	Minimum T	Mean	Trend
Humboldt Gl.	4.9° C	-61.4° C	-26.1° C	0.09° C a^{-1}
Summit	-0.5° C	-59.4° C	-29.6° C	-0.07° C a^{-1}
Tunu-N	3.7° C	-59.0° C	-27.7° C	0.11° C a^{-1}
South Dome	5.2° C	-53.2° C	-19.3° C	0.02° C a^{-1}
NASA-E	4.6° C	-57.7° C	-27.9° C	0.02° C a^{-1}
NGRIP	2.5° C	-68.1° C	-28.4° C	0.13° C a^{-1}

* Italics indicates significant trend ($p < .01$)

3.2. Modeling of Englacial Hydrology

3.2.1. Introduction

The development of large melt ponds on the Greenland Ice Sheet (GIS) and their drainage system indicate that moulins are a major contributor to the englacial water system. Here we review the current state of knowledge and the history of moulin research. In the late 19th century glaciologists led by Vallot climbed and studied the Grand Moulin on Mont Blanc. Despite being considered mystic due to their size and water drainage they have been studied by a few scientists such as *Holmlund and Hooke* (1983) or *Badini and Puccini* (2002). We develop a qualitative model of geometry as well as of the driving forces in the life cycle of moulins using data, photos, sketches, and climbing reports by ice speleologists and climbers.

The GIS is temperate for the first 10 km at its margin and consists of cold ice further inland. The recent increase in melt water leads to an increase in basal water availability. The observed increase in ice velocity might be caused by the lubrication at the bed combined with a possible temperature rise in the cold part of the GIS. The raise of englacial water flow increases the volume of the conduits thus reducing the timing of water to reach the ice sheet bed. Our initial model starts with a narrow englacial non-arborescent channel network. We anticipate the development of the englacial hydrology system by using the 'Roethlisberger' conduit model.

3.2.2. Motivation

Moulins are the gateway to the englacial water system. Despite their impressive size and look they have not been studied in great detail so fare because they were considered to play a minor role in glacier dynamics. This changed with the publication of a paper by *Zwally et al.* (2002) in which they indicated that there may be lubrication at the bed of the GIS. The englacial water system and the moulins have become an interesting subject which needs to be investigated:

- What influences the geometry of a moulin? Is the basal stress or a change of physical properties the reason for the step function geometry? How do the processes differ between cold ice and temperate ice?
- All melt water reaches the ocean at some point, but how? Does the englacial conduit system develop each year or is its lifespan inter-annually? Is water stored in the glacier inter-annually? Can water penetrate through 1100 m of ice within one year and cause lubrication at the bed? How far can the water influence the ice temperature?

These questions shall be answered in the upcoming years while we develop this glacier hydrology model.

3.2.3. Source of water

The false colored near infrared image of the Jakobshavn Isbreae (Fig. 3.2.1) was taken on June 18th, 2003. The first red line from the upper right corner indicates approximately the equilibrium line. The upper part of the ablation zone between the two red lines consists of a large number of superglacial lakes whereas the lower part of the ablation zone is virtually lake free despite melt occurring in the entire area. This indicates that the two areas have different runoff regimes. In the lower zone where most of the moulins are to be found the surface runoff has connected to the englacial water system and to the basal water network.

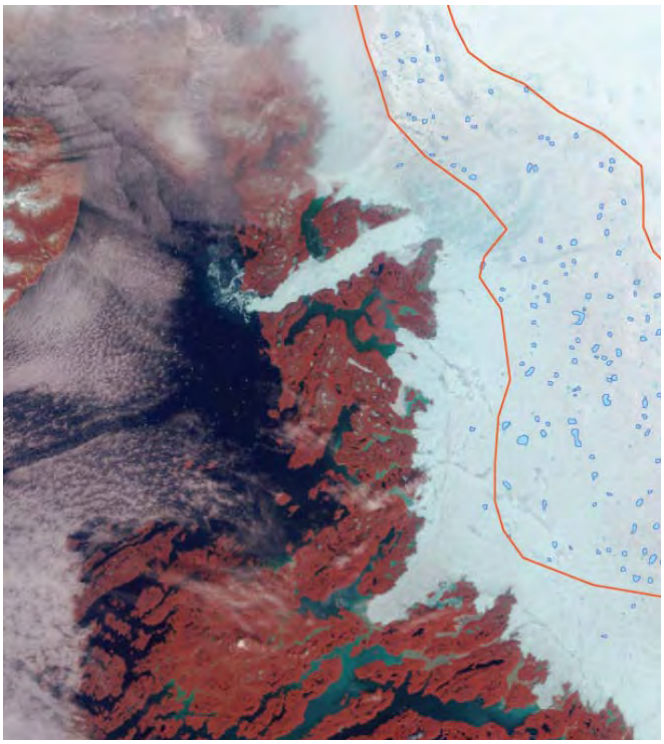

Figure 3.2.1: False color infrared image of the lake distribution for Western Greenland on June 18th, 2003. This image was taken from the NASA homepage. The lakes were identified using ENVI and illustrated in ArcGIS.

Lakes are expected in the lower ablation zone (LAZ) at the beginning of the season. The englacial water network of the previous season has closed up due to ice dynamics caused by the ice velocity as well as a lack of running melt water during the winter months. Previous observations suggest that similar runoff networks are used every season. Our hypothesis suggests that the development of moulins is caused by water inflow into existing crevasses. The pressure caused by standing and flowing water, as well as the increased heat flux through the water, force the moulin to grow in size and connect to the already existing englacial water network. The source of melt water is the motor that drives the glacier hydrology. We intend to make further studies of the changes of the temporal as well as spatial distribution of surface lakes, and compare them to the extent of the englacial network.

The melt area has increased in the past 30 years (Fig. 3.2.2). The amount of water reaching the ocean en- and sub-glacially has increased as a result. Does this influences the volume of the englacial conduits and possibly the ice temperature of the GIS at its margin?

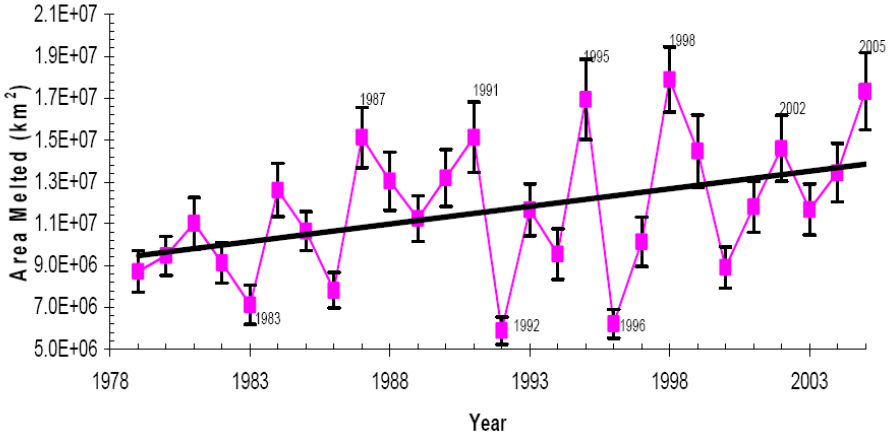

Figure 3.2.2: Total area experiencing melt during each annual melt cycle summed from April 1 through October 31. Error bars represent the 95% confidence interval. Passive microwave was used to measure the melt extent. This data was analyzed by Russell Huff of CIRES.

3.2.4. West Greenland temperature profile

A number of weather stations in the Jakobshavn area have been recording temperature, wind, radiation and snow temperature for more than 10 years. Deep ice temperature profiles were measured by *Thomsen et al.* (1992) in the late 80's and early 90's.

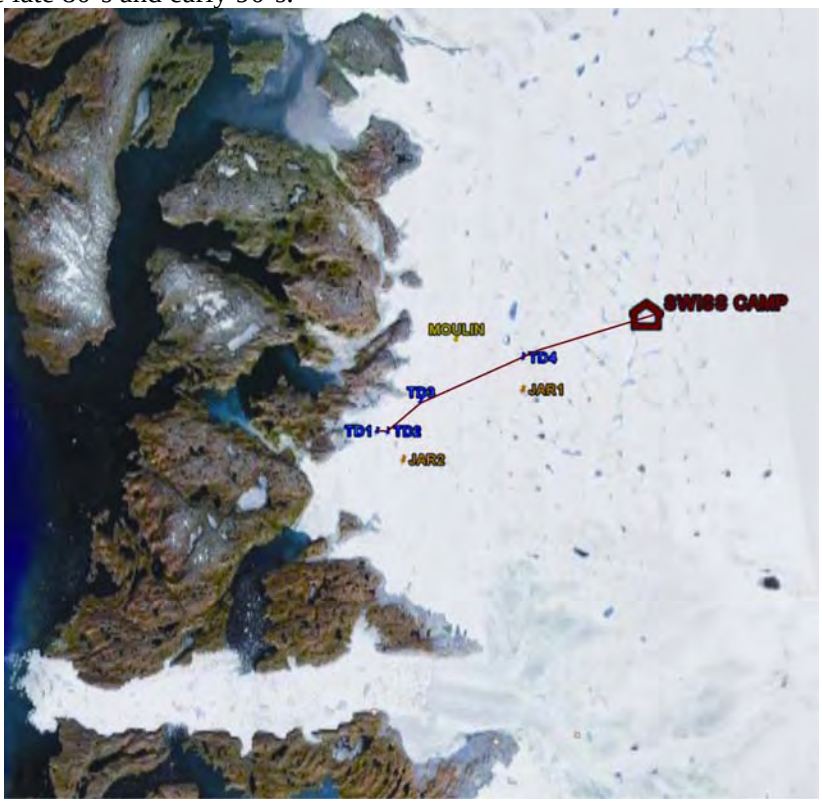

Figure 1.2.3: Google Earth image of the Jakobshavn and Dead Glacier area. TD1 through TD4 are the locations of the temperature profiles in Figure 3.2.4. JAR 1 and 2 are the automatic weather stations which are part of the GC-Data network The moulin located in the image has been visited and studied in 2006 and 2007.

Temperature profiles are shown in Figure 3.2.4 for the marginal ice region of GIS. The rise in temperature is due to frictional heating as the ice dynamics increase towards the edge. The increase may be amplified by the increase of englacial water flow due to a longer melt season and a higher intensity of melt.

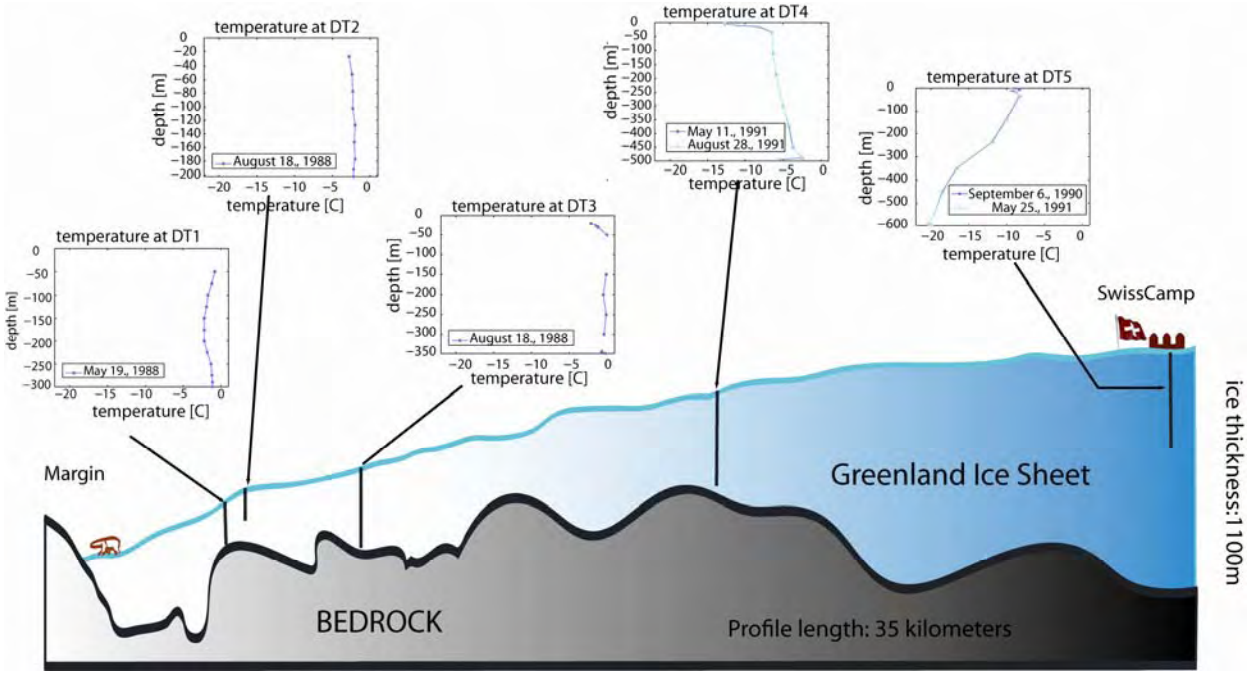

Figure 3.2.4: Temperature profile for transect along Dead Glacier north of Jakobshavn Isbrae. The ice at the margin consists of temperate ice. The GIS is cold ice further inland. The transition zone is very short.

3.2.5. Modelling sub- and englacial conduits

Any physical process involving the phase change of a medium can be simulated by using the Stefan Problem. We use the Fourier heat transfer law to simulate ice melt:

$$c*\rho*\partial u/\partial t = k*\partial^2 u/\partial x^2$$

where c=specific heat, k= heat conductivity and ρ =density. The latent heat loss is:

$$-\lambda*\rho*w*d\xi(t)/dt$$

where λ is the latent heat and ξ the enthalpy.

We started out with a simple steady state problem as depicted in the Figure 3.2.6a. We assume the moulin has standing water that melts the underlying ice. At the surface the water has a constant temperature of 1 ºC, and melts its way into the ice.

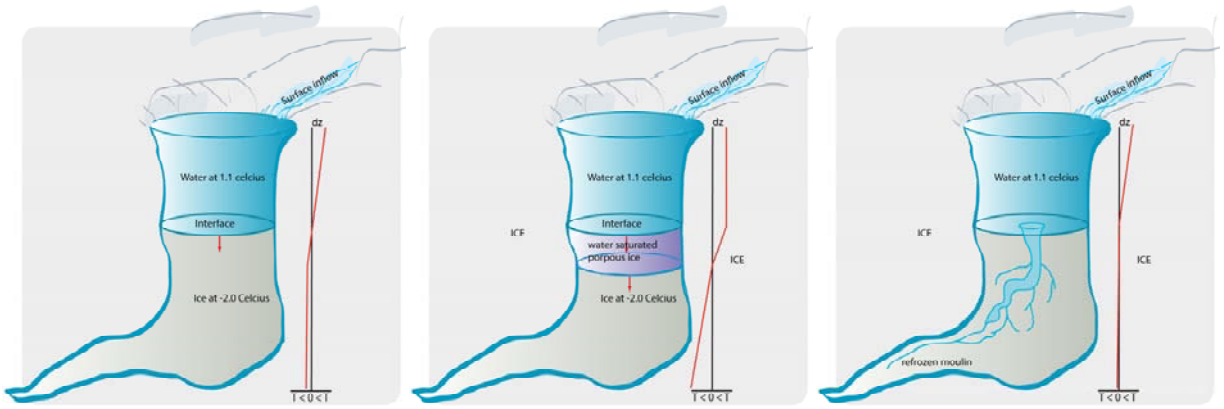

Figure 3.2.6 a) The first approach with standing water and a two dimensional interface between water and ice. b) A porous saturated interface between the water filled Moulin and the ice bellow. c) Fractures in the ice predefine the route taken by the melt water and construct the shape of the Moulin.

The heat flux is a function of the temperature, the latent heat loss a function of enthalpy. In the enthalpy method, which is ideally suited for problems with phase change, the heat equation is written as:

$$\partial / \partial t *(\rho *H/k) - \partial^2 T / \partial x^2 = 0$$

where ρ is the density of the material, H is the enthalpy equals ρ Cp T in the absence of phase change, so the equation reduces to the standard heat equation.

Figure 3.2.6b shows the sketch for the assumption that the physical properties of the ice are not homogeneous: The ice structure is porous which allows the water to infiltrate the ice more easily, resulting in a saturated porous ice layer. The melt route is therefore somewhat predefined. In figure 3.2.6c shows a sketch with already existing channels: The ice has numerous fractures caused by ice dynamics, allowing meltwater to penetrate more easil. Once the fractures get connected and water starts to flow, the network starts to develop conduits.

For the model we intend to use the *Roethlisberger* (1972) algorithm. This attests that increase or decrease of the conduit diameter is the result of the ice pressure versus the water pressure within the conduit. The rate of melt of freezing of a conduit is due to its diameter size as well as the amount of water flow. If the ratio of the water-ice-interface divided by the amount of water within a unit is smaller than the same ratio for the surrounding conduits then the conduit will grow at constant pressure whereas the other conduits will start to close up. A non-arboresque network will develop into an arboresque network with main water channels. The result will be an englacial water network system.

The model will be based on the assumption that the glacier contains of fractures which are connected by tiny conduits so water flow can start (Fig. 3.2.7). The resulting networks will be analyzed and compared to field data collected using ground penetrating radar to detect the conduits and the moulins as shown in Figure 3.2.7.

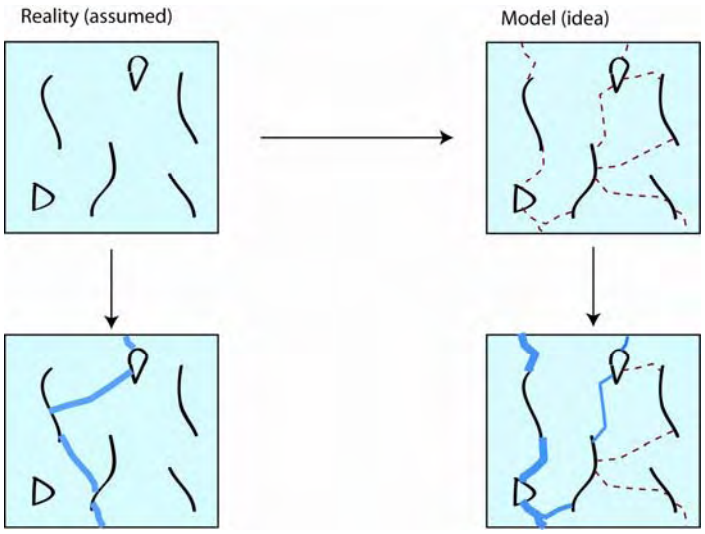

Figure 3.2.7: Fountain et al. (2005) discovered fractures right to the base in Storeglaciaren glacier in Sweden. We make the same assumption for Greenland: There are fractures and voids in the ice as a result of the ice dynamics, which make the glacier a porous media allowing the water to penetrate through the glacier faster and creating an englacial network.

3.2.6. Preliminary results for melt

The changes of temperature for each time step were calculated using the Euler Backward method to solve numerical problems. The Euler Backward was calculated using Newton's method:

$$[F] * \partial T = -f(T(n))$$

$$T(n+1) = T(n) + \partial T$$

where *F* is a Jacobi matrix for *f*' for each depth. The first two graphs are for short time periods and shallow depth. In Figure 3.2.8b the break in the curve at the melting point is clearly visible for each time step. For a steady state assumption where the temperature at height zero is held at 1 ºC up to 20 cm of ice can be melted in 3 hours.

In Figure 3.2.8a the temperature profiles for each time step are shown. The heat flux at depth x = 1m is $\partial T / \partial x = 0$. This results in the ice temperature increases rapidly over time. In Figure 3.2.8a a diurnal cycle has been included and simulated for three days. The temperature flux at 30 m depths has been set to T(in) =T(out). The assumption is that the temperature at this depth is not influenced by the surface change for this short period of time.

The result though indicates that the energy loss is too large as the depth of the melt interface is slowed down over this time. The standing water, which changes its temperature between 0.1 ºC and 1.1 ºC at depth x = 0, melts 75 cm of ice over three days according to the model. This does not include any frictional heating.

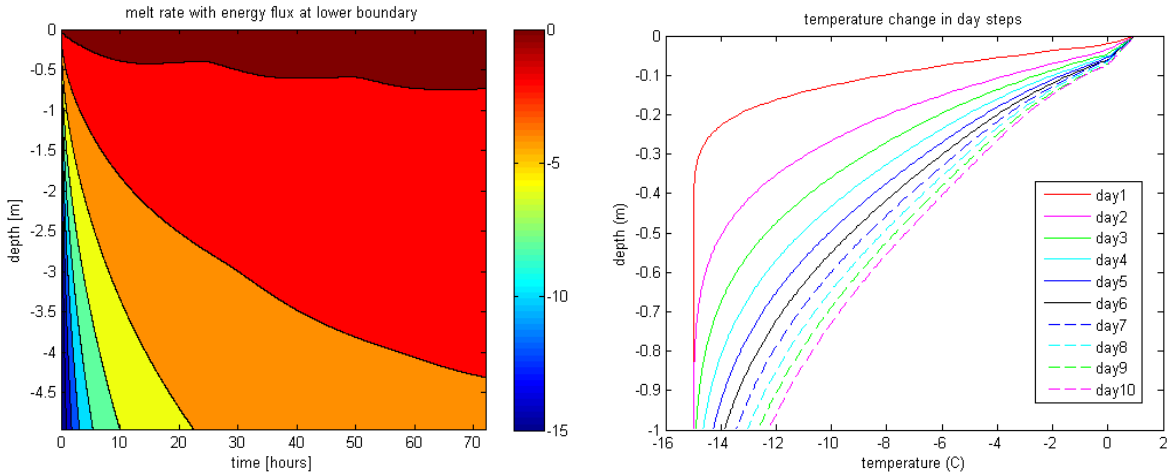

Figure 3.2.8a: Change of temperature in the top 4.5 m of ice over 3 days. The ice is assumed to be -15ºC at time step 1. The temperature at the surface varies between 0.1 and 1.1 ºC. The dark red is the depth of water. The water temperature changes in a diurnal cycle but never refreezes. Figure 3.28b shows the temperature curves at various time steps. There is a very distinctive break at the melting point.

The model makes the assumption that the melted water does not refreeze. This is certainly not correct at the beginning of the melt season but is plausible for an established super-glacial lake. These are obviously preliminary results. Further research will give us the possibility to improve our model.

3.3 Influence of Meltwater on Greenland Ice Sheet Dynamics

3.3.1 An overview of the importance of water in ice dynamics

Paleo ice sheet glaciohydrology may have been responsible for producing Heinrich layers, through periodic cycles of enhanced ice flow. Glaciohydrology may have also been a key contributor to the eventual demise of paleo ice sheets, such as the Scandinavian ice sheet (*Arnold and Sharp*, 2002). As a result of concerns over contemporary sea level rise and ice sheet stability, the influence of meltwater on the ice dynamics of the Greenland Ice Sheet is a highly topical branch of cryospheric research. Located near the equilibrium line, with abundant surface meltwater, Swiss Camp, Greenland, provides an ideal location to study the influence of meltwater on ice dynamics (*Steffen et al.*, 2004; Figure 3.3.1). Currently, a pressing question is whether or not surface meltwater, which is typically produced at a rate of one to three orders of magnitude greater than basal meltwater, reaches the bed of the Greenland Ice Sheet. The presence of water is thought to potentially enhance each of the three mechanisms through which ice flows: (i) internal deformation, (ii) basal slide and (iii) basal sediment deformation.

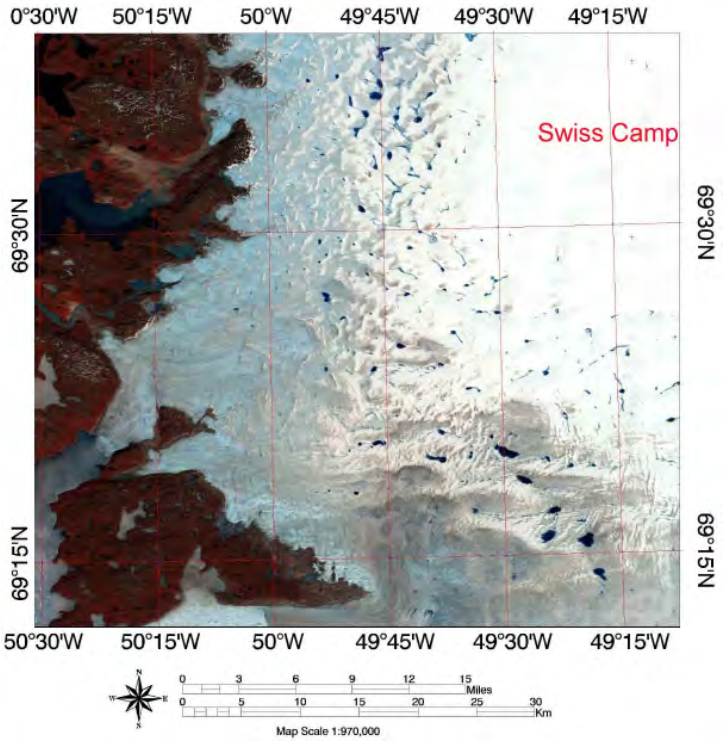

Figure 3.3.1: Swiss Camp, on the western margin of the Greenland Ice Sheet, has abundant surface meltwater in its vicinity, making it an ideal study site to investigate the influence of meltwater on ice dynamics.

Internal deformation of an ice mass is described by the Glen Flow Law:

$$\varepsilon = B\sigma^n$$

where ε and σ are the strain and stress rates respectively, *B* is the Glen law parameter (representing viscosity) and *n* is the dimensionless Glen law exponent (*Glen*, 1958). When $n = 1$, strain is linearly proportional to stress, with a constant of proportionality of *B*. In ice however, *n* is typically taken to be ≈ 3, to represent deformation via a non-linear viscosity-dependent power law function (*Marshall*, 2005). The viscosity parameter (*B*) is highly temperature dependent. Effective viscosity is believed to be vary between 10^{11} and 10^{17} Pa s over the temperature range of -2 to -32 °C in the Greenland Ice Sheet (*Marshall*, 2005; Figure 3.3.2). As moulins effectively channel meltwater, and the latent heat contained within, into the englacial hydrology system, increased meltwater production in the marginal areas of the Greenland Ice Sheet will result in increased energy transport into ice sheet. Over time, this process may potentially warm marginal areas of the Greenland Ice Sheet, thereby reducing viscosity.

Basal flow occurs when subglacial water reduces basal friction by lubricating or floating an ice mass over the bed surface. Although basal meltwater has traditionally been thought to be the primarily source of subglacial water, models have recently shown that supraglacial streams with discharges of over 0.15 m^3 s^{-1} can theoretically penetrate down through 300 m of ice to reach bedrock, via self-propagation of water filled crevasses (*Arnold and Sharp*, 2002; Figure 3.3.3). There are several possible subglacial hydrological configurations: ice-walled conduits, bedrock conduits, water film, linked cavities, soft-sediment channels, porous sediment sheets and ordinary aquifers (*Mair et al.*, 2001; *Flowers and Clarke*, 2002). Each of these configurations achieves a different maximum subglacial water pressure. Subglacial water pressure directly influences basal flow according to:

$$v = C\,\gamma\,\sigma'$$

where v is the basal velocity, C is a sliding law parameter and σ' is the deviatoric stress tensor. As the flotation fraction (γ) is defined as the ratio of subglacial water pressure to overburden ice pressure, enhanced basal flow can be expected as a result of increased subglacial water pressures (*Marshall et al.*, 2005). When an ice mass is in long term equilibrium, the volume of surface meltwater reaching the subglacial system may be assumed to be constant. As the surface melt in the marginal areas of the Greenland Ice Sheet increases beyond long term equilibrium however, a greater volume of surface meltwater may be expected to reach the subglacial system in marginal areas, increasing the floatation fraction in these regions.

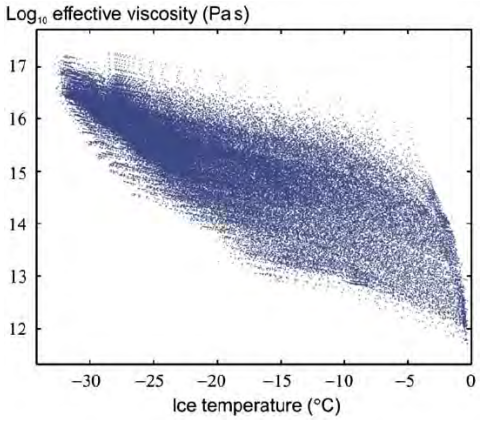

Figure 3.3.2: The modeled effective viscosity of ice versus temperature in the Greenland Ice Sheet (Marshall, 2005). Warmer ice is less viscous than colder ice.

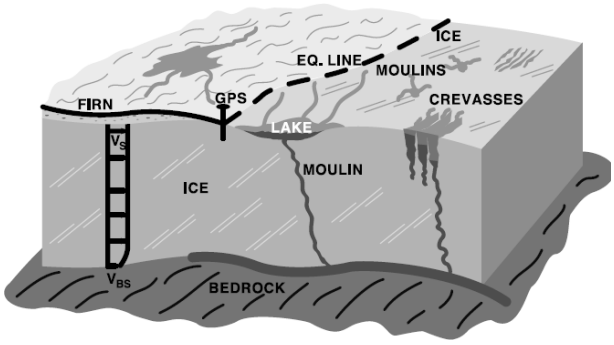

Figure 3.3.3: Schematic illustrating the routing of surface meltwater to the subglacial system (Zwally et al., 2002). Increased subglacial water can enhance basal slide.

Similar to basal flow, basal sediment deformation can also be enhanced by the presence of increased subglacial water. The failure of basal sediment along a given shear plane can be described as:

$$\tau_f = c + (\sigma_n - p_w) \tan\theta$$

where τ_f is the shear strength of failure, c is the apparent cohesion of basal sediment, σ_n is the normal stress, p_w is the basal pore pressure and $\tan\theta$ is the internal friction angle (*Tulaczyk et al.*, 2000; Figure 3.3.4). Increased subglacial pore water pressure results in decreased effective normal stress (approximated by $\sigma_n - p_w$). This subsequently lowers the shear strength of failure of the basal sediment, allowing greater basal sediment deformation and a greater contribution to ice velocity.

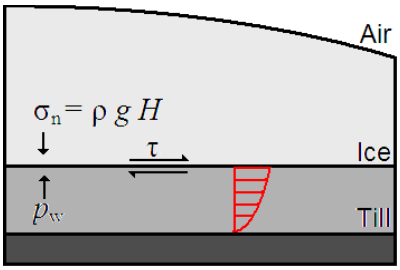

Figure 3.3.4: Schematic of the forces controlling the shear strength of failure in basal sediment. A theoretical basal deformation profile is shown (red). Basal sediment deformation can be enhanced through the presence of increased subglacial water.

3.3.2 Evidence of subglacial water in the Greenland Ice Sheet

The mass balance of the Greenland Ice Sheet is controlled by both its surface balance and its ice dynamics. Previous NASA-funded research has found ice flow in west-central Greenland to accelerate during periods of summer melting, followed by a deceleration after melt cessation. An apparent relation between ice acceleration and the duration of summer melting has been interpreted as evidence of enhanced by basal slide due to the rapid channeling of surface meltwater to bed during melt periods (*Zwally et al.*, 2002; Figure 3.3.5). Similar studies in other regions of the Greenland Ice Sheet are lacking at this time, and therefore the prevalence of this phenomenon is not completely known.

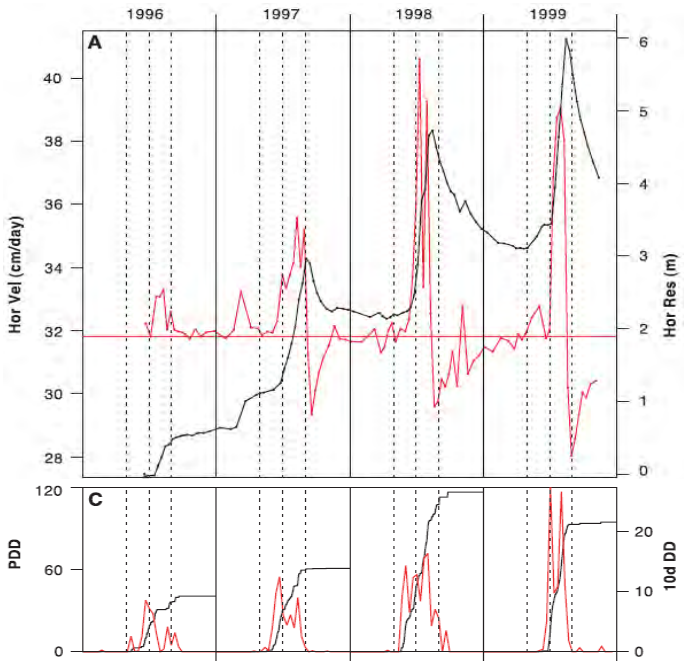

Figure 3.3.5a: Cumulative motion (black) and horizontal ice velocity (red) showing ice accelerations during the summer melt seasons and abrupt transitions to deceleration around the times of melt cessation. (c) Cumulative positive degree days (PDDs) and PDDs for 10-day intervals (10d DD; red) at Swiss Camp (Zwally et al., 2002). The rapidity of the onset and cessation of events suggests surface meltwater is being rapidly channeled to the subglacial system.

Naturally, the presence of subglacial water requires warm-based conditions. Recent modeling suggests that the majority of the marginal area of the Greenland Ice Sheet is indeed warm-based (*Marshall*, 2005; Figure 3.3.6). As a result of steep surface slopes, these marginal areas have relatively high driving pressures, which subsequently leads to relatively high internal heat production through internal deformation. This frictional heating is believed to be responsible for up to 0.5 m a^{-1} of basal melt in regions of thick ice and steep surface slopes such as Jakobshavn Isbrae on the west coast of Greenland (*Marshall*, 2005). The lack of driving stress under the ice divides of the Greenland Ice Sheet results in little deformational heating and cold-based conditions (*Marshall*, 2005).

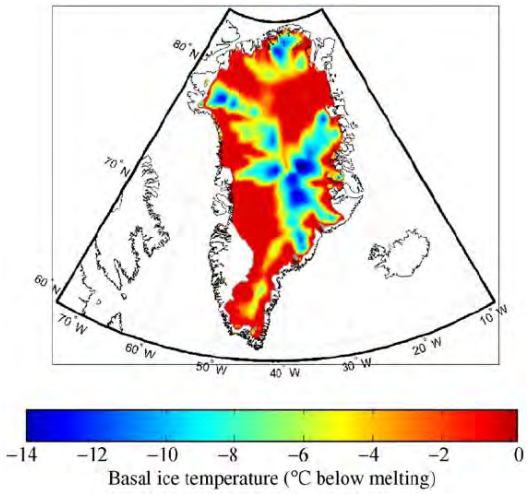

Figure 3.3.6: Modeled present-day basal temperature, corrected for melting point depression due to overburden pressure, in the Greenland Ice Sheet (Marshall, 2005). Widespread warm-based conditions allow the possibility of widespread subglacial water.

3.3.3 An introduction to the Swiss Camp Regional Model

Unfortunately, it is almost impossible to empirically observe the channels and storage compartments which compose the Greenland Ice Sheet's englacial and subglacial hydrology systems. Therefore, numerical models are currently one of the best tools available to study meltwater routing and the structure of englacial and subglacial systems. Glaciological models have only relatively recently begun completely couple ice dynamics and hydrology (composed of supra-, en-, sub-glacial and groundwater hydrology). Archived GC-Net, laser altimetry and GPS data collected during previous NASA-funded field campaigns, as well as moulin structure data obtained during the 2007 field season, is being incorporated into a regional-scale coupled ice dynamic-hydrology model of the Swiss Camp region. The aim is to develop a well-constrained model of high spatial and temporal resolution that is able to predict future changes in ice sheet geometry in the Swiss Camp region, as well as project both short and long term sea level rise contributions from the region. This model is being compiled at the Cooperative Institute for Research in Environmental Science (CIRES) at the University of Colorado by a PhD candidate (William Colgan) under the supervision of Dr. Konrad Steffen. Programming commenced in September 2007 and is scheduled to finish in September 2009, allowing two field seasons to collect calibration data at Swiss Camp.

The model domain is centered around Swiss Camp, extending approximately 150 km along the western margin of the Greenland Ice Sheet (from 68.75 to 70.25 °N), and approximately 300 km inland from the ice sheet margin towards the main drainage divide (from 41.72 to 50.95 °W; Figure 3.3.7). This domain includes the majority of the terminal portion of the Jakobshavn Isbrae drainage basin, the largest drainage basin of the Greenland Ice Sheet. Only a small region of the Greenland Ice Sheet is being modeled due to computational limitations. Time iterations will be calculated using finite difference approximations. Sensitivity and calibration experiments are planned at a variety of time steps (from 1 day to 1 year) to find the most efficient (longest) time step that accurately models observations. Similarly, experiments will be executed using a variety of grid sizes (from 50 m to 3 km) to find the most efficient (largest) grid size that accurately models observations. By using highly efficient numerical methods to update grid cells, such as successive over-relaxation, we expect a model capacity of between 1,000,000 and 10,000 degrees of freedom per time step (where 'degrees of freedom' is the product of the number of grid cells and the number of variables in each cell).

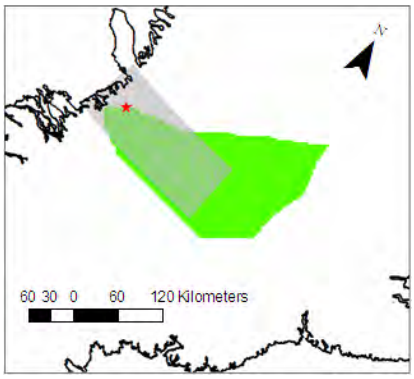

Figure 3.3.7 The domain of the Swiss Camp Regional Model (grey) shown with the approximate outline of the Jakobshavn Isbrae drainage basin (green). Swiss Camp is identified with a red star.

The Swiss Camp Regional Model is initialized with geometry and climatology datasets. From these initial datasets, both surface balance and ice dynamics are derived. An evolving mass balance model is employed, in which the surface balance of each grid cell is calculated from climatology datasets, such as air temperature and precipitation (drawn from GC-Net), according to latitude, longitude and elevation (*Box and Steffen*, 2001). Although the three-dimensional ice dynamic model is based on the shallow ice approximation, in also incorporates the effects of longitudinal coupling, as these forces are significant in the shallow marginal area of the ice sheet. Initial geometry datasets include surface and bedrock topography in the Swiss Camp region. In comparison to the bedrock topography, the ice surface topography in the Swiss Camp region is relatively simple (*Bamber et al.*, 2002; Figure 3.3.8). Although the bedrock topography is complex, it is representative of large areas of the Greenland Ice Sheet, as the bedrock elevation generally increases from well below sea level at the centre of the ice sheet to well above sea level at the margin.

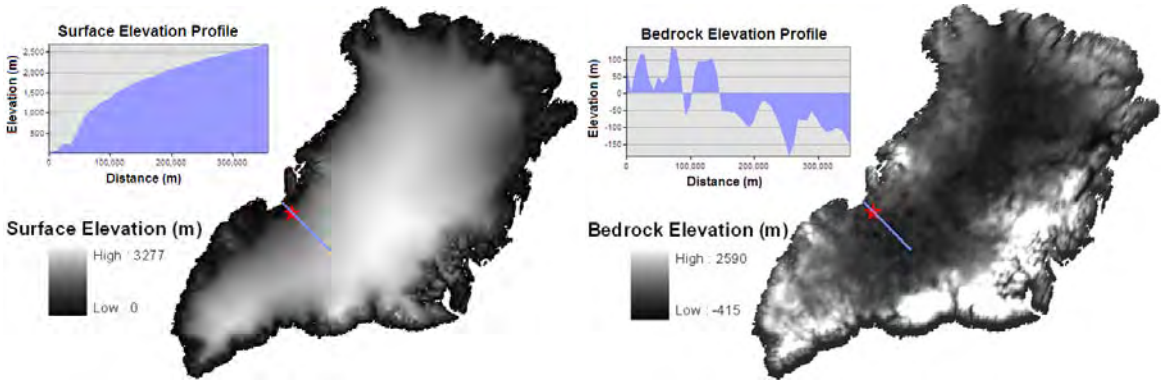

Figure 3.3.8: Surface (left) and bedrock (right) topographies near Swiss Camp (red star; Bamber et al., 2001).

Currently, the Swiss Camp Regional Model uses idealized surface and bed topographies derived from a previously published digital elevation model (*Bamber et al.*, 2002; Figure 3.3.9). Unfortunately, most previously published surface elevation models suffer from reduced accuracy in the marginal areas of the Greenland Ice Sheet, in comparison to the interior of the ice sheet. Developing high-resolution digital elevation models of surface and bedrock topography is a priority for our group at this time. Previously obtained NASA laser altimetry flightlines will be the foundation of the Swiss Camp region surface elevation model (*Abdalati and Krabill*, 1999).

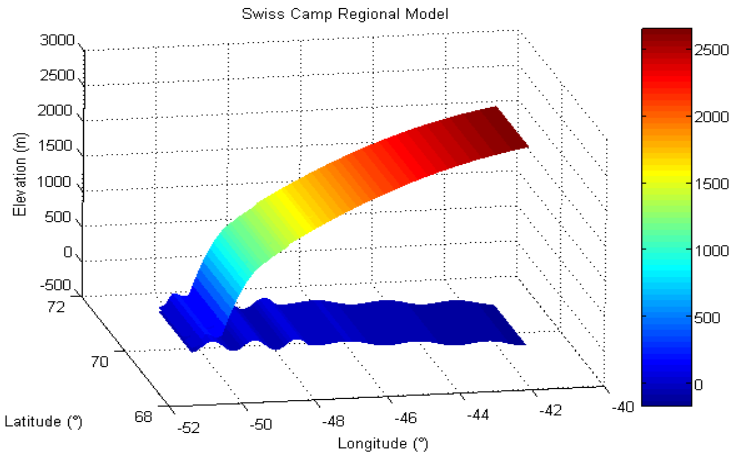

Figure 3.3.9: Idealized surface and bedrock topographies of the Swiss Camp Regional Model are representative of large areas of the ice sheet (Figure 3.3.8).

The hydrological portion of the model simulates the exchange, storage and transport of water between the supra-, en-, sub-glacial and groundwater systems (*Flowers and Clarke*, 2002). Each of these four hydrology systems is modeled by an independent set of equations which allow communication with the other hydrology systems (*Flowers et al.*, 2005). Modeling the storage volume and transport efficiency between systems benefits greatly from the moulin field work performed at Swiss Camp in 2007. Despite the inevitable lack of englacial and subglacial field data, a main advance of this coupled model will be that enhanced basal slide in the Swiss Camp region can now be simulated in a physically-based fashion, using equations to explain either reduced friction through meltwater lubrication or the deformation of basal sediment, rather than being parameterized as in the past. Surface meltwater production, the main control of glaciohydrology, driven by positive degree day modeling, also makes uses of archived GC-Net data (*Box and Steffen*, 2001). Projected future increases in meltwater production will be modeled by forcing the reference GC-Net climatology with the 3 to 6 °C warming predicted for the Swiss Camp region by the year 2100 (*ACIA*, 2006).

The relatively high quality of datasets previously collected in the Swiss Camp region make it a unique area in which to construct a well constrained model of high spatial and temporal resolution and address the pressing question of whether or not surface meltwater reaches the bed in this portion of the Greenland Ice Sheet. Once completed, the Swiss Camp Regional Model will allow the relative contributions of internal deformation, basal slide and basal sediment deformation to ice flow velocity to be elucidated along a portion of the western margin of the Greenland Ice Sheet. The effects of projected future increases in surface meltwater production on each of these processes can then be predicted, allowing future ice flow velocities and sea level rise contributions to be forecast on a variety of timescales. The model will have sufficient flexibility so as to allow the possibility of using entire ice sheet climatology and geometry, should computational resources become available in the future.

3.4 UAS over the Greenland Ice Sheet

3.4.1 Overview

Incorporating new technologies to obtain unique data sets is key to furthering our understanding of changes to the Greenland Ice Sheet. Using sensors such as hyperspectral imagers and synthetic aperture radars at high resolution with multiple frequent revisit times will allow for more complete change-detection and monitoring. Recent advances in Unmanned Aircraft Systems (UAS) show promise for in-

novative data collection over the ice flows, crevasses, and other difficult-to-access locations. At the end of the 2007 summer field season, an opportunity was available to demonstrate the use of a few Unmanned Aircraft Vehicles (UAV's) to gather multi-mode scientific data over the ice sheets and surrounding glacially-carved valleys. The UAV's and their sensors flew eight flights during one week, August 21st to August 26th, 2007, in the vicinity of Kangerlussuaq International Airport. The Figure 3.4.1 shows the location of the operational flight area (red box), the UAV transition flight line (purple), and the approach/departure into the international airport (green line).

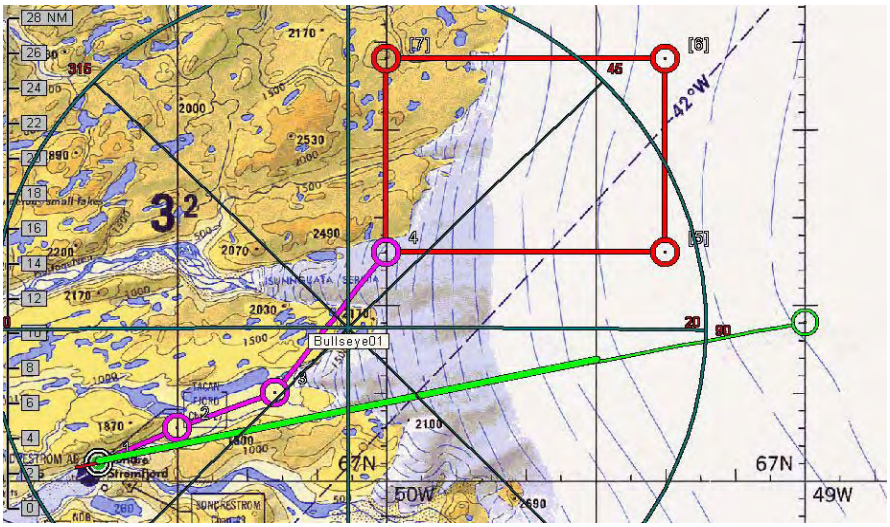

Figure 3.4.1: Location of operational flight area (red box), UAV transition flight line (purple) and the approach/departure into the international airport (green line)

3.4.2 Data collection platforms

Two UAV platform types were flown, the Manta (Fig. 3.4.2) and the Silver Fox (Fig. 3.4.3), both manufactured by Advanced Ceramics Research of Tucson, Arizona. The Silver Fox was flown with two different engine types: an innovative electric engine, and the traditional gas engine. Both platforms are fairly small (six foot wing spans), portable, and can be field launched.

Figure 3.4.2 Manta UAV

Figure 3.4.3: Silver Fox UAV

Flight Dates and Mission Profiles:

08/21/07	Silver Fox	Gas engine test and checkout
08/22/07	Manta	Test and checkout

08/22/07	Manta	Hyperspectral flight
08/23/07	Silver Fox	Electric engine test and checkout
08/24/07	Silver Fox	Electric engine camera imaging flight
08/25/07	Silver Fox	Two electric engine SAR flights
08/26/07	Silver Fox	Electric engine camera imaging flight

3.4.3 Sensors

The field-testing involved three sensor types: hyperspectral imager, a Synthetic Aperture Radar (SAR), a standard digital camera. The first objective was to fly with the hyperspectral imager over supraglacial lakes that appear on the tops of the glaciers. By analyzing the reflected solar energy of 60 discrete spectral bins, it is theorized the bottom depths can be computed. The pixel resolution was excellent, 0.4 m x 0.56 m when the UAV is flying at 1000 feet above ground level (AGL); the swath width is 90 meters. Using the depth calculations and the surface area measurements, the total liquid water volume can then be calculated. An accurate lake volume is important for improving glacial hydrologic models, as these lakes can drain in timeframes of less than one day.

3.4.4 Data discussion

An example of one of the data cubes from the hyperspectral sensor is shown in Figure 3.4.4. Three of the 60 channels are shown, along with an image of the flight track at the bottom of the figure. When reviewing the UAV track from left to right, one can see the white ice, followed by the shore of the supraglacial lake, then the darker waters of the deeper middle lake segment, the lighter waters of the shoreline on the other side, and finally the white of the ice as it rises in elevation again. Looking at the spectral graph, one notices the decrease in attenuation of light from 530 nm to 461 nm, then the increase in attenuation again between 461 nm to 409 nm.

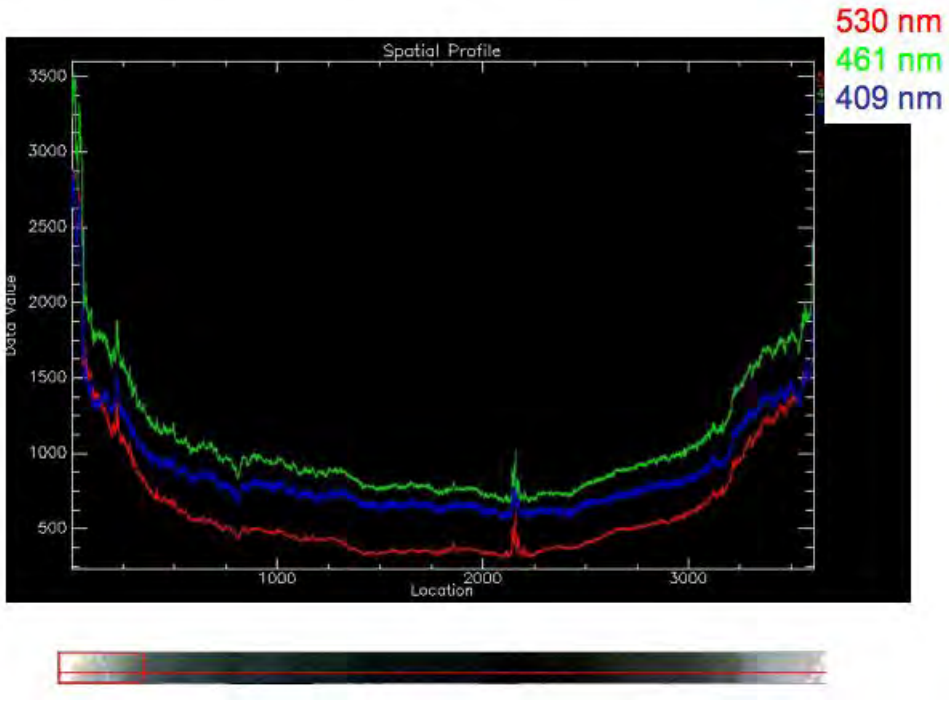

Figure 3.4.4: Spectral reflectance (530 nm in red, 461 nm in green, and 409 nm in blue) along the UAV flight track of a melt water lake on the Greenland ice sheet.

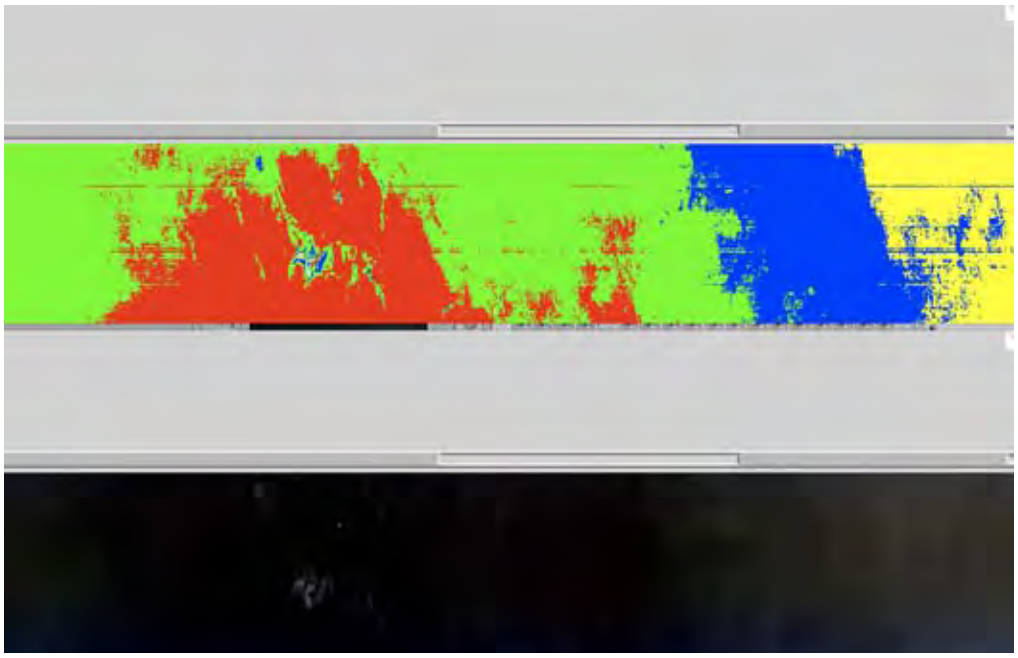

Figure 3.4.5: Supervised classification of surface types using hyperspectral sensor data

The hyperspectral data was also used in a classification schema using ENVI software to produce a contour map of the bottom depth. A sample of the output is shown below. Although it is difficult to notice the depth changes visually, using the spectral characteristics of the returns, it was possible to map the depths using this passive technique.

A second objective was to obtain SAR data in conjunction with imagery. The SAR data can be used for ice crevasse mapping and the determination of leads in sea ice. This data is important for developing models of ice dynamics and its response to climatic changes.

3.4.5 Conclusions

This project was successful in many respects: it demonstrated that scientific UAS missions could be flown from the main International Airport in Greenland, proved the viability of an electrically powered UAV as a SAR or imagery platform, showed that hyperspectral imaging of supraglacial lakes can be used for depth characterizations, and demonstrated how small, field-launchable UAV's can be launched and recovered in the arctic environment. This project further illustrated that international cooperation can allow autonomous unmanned data collection platforms to be used in the pursuit of new scientific knowledge. The combination of these attributes could be extremely useful in future satellite calibration and validation efforts such as Cryosat 2.

Figure 4.4.6: Graduate student John Adler with Manta UAV after a successful landing in the sander of Kangerlussuaq, Greenland..

3.4.6 Future research

Future scientific work would include optimizing an algorithm for supraglacial lake depths, the addition of a green or blue wavelength laser altimeter for point depth measurements (up to ~10 m depths), and/or the development of a 10-13GHz radar altimeter for the determination of snow depths over ice (either sea ice or glacial ice).

4. Proposed Field Activities and Research Objectives 2008

4.1 AWS Maintenance

The automatic weather station network will be maintained. In the north, the Petermann ELA stations will be serviced as part of the NSF/NASA supported field activities. We will visit the new NEEM AWS to download the data and relocate the station to close to the new drilling camp. Further, GITS, Hum, Tunu-N, NASA-SE, NASA-U, NGRIP, and Summit will be serviced. The profile JAR2, JAR1, CU/ETH, and Crawford 1 will be serviced while at the Swiss Camp. In the southern part of the ice sheet we will service the DYE-2, Saddle, NASA SE, and Saddle (Fig. 1.1) to reactivate the satellite transmitter, download the data and collect snow stratigraphy information.

The field season 2008 will concentrate to upgrade all existing AWS's on the Greenland ice sheet with updated data loggers and some new instrumentation. Further, we will install new GPS unites for those AWS's that transmit via GOES satellite and need a very accurate time stamp. Several AWS's have melted out in the ablation region near Swiss Camp and need to be re-drilled. The surface melt in summer 2007 exceeded all previous records.

4.2 GPS Network Maintenance

Our effort to monitor the ablation along a transect from the Swiss Camp to the ice margin will continue. We will service the GPS network in collaboration with Dr. Jay Zwally (NASA-GSFC) and will add two new GPS monitoring stations in the Jakobshavn region. We will continue to collect high-resolution surface topography data using Trimble Pathfinder differential GPS measurements along several transects in the lower ablation region. In addition, we will acquire a sequence Landsat TM satellite imagery during the onset of melt and melt period to monitor the spatial variation and extent of snow fields in the ablation region.

4.3 Ground Penetration Radar

We have collected a number of ground penetrating radar (GPR) profiles along the western slope of the ice sheet (Jakobshavn and Kangerlussuaq region) in previous field seasons (1999, 2000, 2003, and 2007). The analysis of this data set showed that the accumulation could vary up to 40% between the trough and the ridge of the undulation. The surface topography with scale length of several kilometers plays an important role for the spatial variability of accumulation, the mass transfer, and the surface energy balance. We will repeat some of these GPR measurements during the spring 2007 field season along the same profiles to verify the recent accumulation changes and high percolation events in that region. We also purchased a new MALA 10 KHz ground penetrating antenna to map the underside of the Greenland ice sheet below Swiss Camp towards the ice margin in view of our moulin modeling. We need to assess the sub glacial conduit density and the occurrence frequency of moulin (relics) in spring 08

5. Bibliography

Abdalati, W., and K. Steffen, Passive microwave derived snowmelt regions on the Greenland ice sheet. *Geophysical Research Letters* 22(7), 787-790, 2001.

Abdalati, W., and K. Steffen, Greenland ice sheet melt extent: 1979-1999. *Journal of Geophysical Research* 106(D24), 33,983-33,988. 2001.

Abdalati, W., and W. Krabill, Calculation of Ice Velocities in the Jakobshavn Isbrea Area Using Airborne Laser Altimetry. *Remote Sensing of Environment.* 67: 194-204, 1999.

Abdalati, W., and K. Steffen, Snowmelt on the Greenland ice sheet as derived from passive microwave satellite data. *Journal of Climate* 10(2), 165-175, 1997.

ACIA: Arctic Climate Impact Assessment Report, Cambridge University Press. doi: 10.2277/0521865093, 2006.

Arnold, N. and M. Sharp, Flow variability in the Scandinavian Ice Sheet: modeling the coupling between ice sheet flow and hydrology. *Quaternary Science Reviews.* 21: 485-502, 2001.

Arthern, R.J., and D. J. Wingham, The natural fluctuations of firn densification and their effect on the geodetic determination of ice sheet mass balance. *Climatic Change* 40, 605-624, 1998.

Badino, G., and L. Piccini, Englacial water fluctuation in moulins: an example from Tyndall Glacier (Patagonia, Chile), *Nimbus, 23-24*, 125-129, 2002.

Bamber, J., S. Ekholm and W. Krabill, A new, high-resolution digital elevation model of Greenland fully validated with airborne laser altimeter data. *Journal of Geophysical Research.* 106: 6733-6745, 2001.

Box, J.E. and K. Steffen, Sublimation on the Greenland ice sheet from automated weather station observations, *J. Geophys. Res., 106*(D24), 33,965-33,982, doi:10.1029/2001JD900161, 2001.

Burns, G.W., M. G. Scroger, G. F. Strouse, M. C. Croarkin, and W. F. Guthrie, Temperature-electromotive force reference functions and tables for the letter-designated thermocouple types based on the ITS-90. Gaithersburg, MD, U.S. Department of Commerce. National Institute for Standards and Technology. (NIST Monograph 175), 1993.

Cathles, L., L.M. Maclagan IV, III Cathles, and M.R. Albert, A physically based method for correcting temperature profile measurements made using thermocouples. *Journal of Glaciology* 53(181), 298-304, 2007.

Flowers, G., and G. Clarke, A multi-component coupled model of glacier hydrology. *Journal of Geophysical Research.* 107-B11: 2287, 2002.

Fountain, A.G. R.B. Schlichting, P. Jansson,and R.W. Jacobel, Observation of englacial water passages: a fracture dominted system, *Annals of Glaciology, 40*, 25-29, 2005.

Glen, J., The flow law of ice. *International Association of Hydrologic Science Publication.* 47: 171-183, 1958.

Holmlund, P., and R.L. Hooke, High water-pressure events in moulins, Storglaciaren, Sweden, *Geografiska Annaler, 65A*, 19-25, 1983.

Herron, M.M., and C.C. Langway, Jr., Firn densification: an empirical model. *Journal of Glaciology* **25**(93), 373-385, 1980.

Holmlund, P., Internal Geometry and Evolution of Moulins, Storglaciaren, Sweden, *Journal of Glaciology, 34*, 242-248, 1988**.**

Kojima, K., Physics of snow and ice. *Contribution* 799**,** *Proceedings of the International Conference on Low Temperature Science, Sapporo, Japan*, 929-952, 1967.

Mair, D., P. Nienow, I. Willis and M. Sharp, Spatial patterns of glacier motion during a high-velocity event: Haut Glacier d'Arolla, Switzerland. *Journal of Glaciology*. 47: 9-20, 2001.

Marshall, S., Recent advances in understanding ice sheet dynamics. *Earth and Planetary Science Letters*. 240: 191-204, 2005.

Recktenwald, G., *Conversion of Thermocouple Voltage to Temperature*. http://web.cecs.pdx.edu/~gerry/epub/pdf/thermocouple.pdf, 2006.

Reynaud, L., The November 1986 survey of the Grand Moulin on the Mer de Glace, Mont Blanc Massif, France, *Journal of Glaciology*, *33*, 130-131, 1987**.**

Röthlisberger, H., Water pressure in intra- and subglacial channels, 11, 177-203, 1972**.**

Schytt, V., The inner structure of the ice shelf at Maudheim as shown by core drilling. *Norwegian-British-Swedish Antarctic Expedition, 1949-52, Scientific Results* 4, *Glaciology 2.* Norsk Polarinstitutt, Oslo, 115-151, 1958.

Schytt, V., Snow and ice temperatures in Dronning Maud Land, Scientific Results, Norwegian-British-Swedish Antarctic Expedition, 4 D, Norsk Polarintitutt, Oslo, 1960.

ShuFman, C., K. Steffen, J. Box, and C. Stearn, A dozen years of temperature observations at the Summit: Central Greenland automatic weather stations 1987-1999, *J. Appl. Meteorol*., *40*(4),741-752, 2001.

Steffen, K. J. Box, and W. Abdalati, Greenland Climate Network: GC-Net. *CRREL Report on Glaciers, Ice Sheets, and Volcanoes*, 96-27, 98-103, 1996.

Steffen, K., A. Nolin, J. White, Assessment of Variations in the Snow Accumulation Rate in Northern Greenland, Annual Progress Report to National Science Foundation. NSF/OPP 9423530, pp.14., 1997.

Steffen, K. and J. Box, Surface climatology of the Greenland ice sheet: Greenland Climate Network 1995-1999, *Journal of Geophysical Research* 106(D24), 33,951-33,964, 2001.

Steffen, K., S. Nghiem, R. Huff and G. Neumann, The melt anomaly of 2002 on the Greenland Ice Sheet from active and passive microwave satellite observations. *Geophysical Research Letters.* 31: L20402, doi: 10.1029/2004GL020444, 2004.

Steffen, K., and J.E. Box, Surface climatology of the Greenland ice sheet: Greenland climate network 1995-1999, *J. Geophys. Res*., 106(D24), 33,951-33,964, 2001.

Tulaczyk, S., W. Kamb and H. Engelhardt, Basal mechanics of Ice Stream B, West Antarctica 1. Till mechanics. *Journal of Geophysical Research*. 105: 463-482. doi:10.1029/1999JB900329, 2000.

Zwally, H.J. and J. Li, Seasonal and interannual variations of firn densification and ice-sheet surface elevation at the Greenland summit. *Journal of Glaciology* 48(161), 199-207, 2002.

Zwally, H.J., W. Abdalati, T. Herring, K. Larsen, J. Saba, and K. Steffen. Surface melt-induced acceleration of Greenland ice-sheet flow, *Science*, 297, 218-222, 2002.